

## ABSTRACT

### **Cu<sup>2+</sup> Binding to A $\beta$ peptides: Detailed Heat Capacity Studies Provide Structural Insight into Complex Formation**

Sunitha Gade

January, 2013

Chair: Rickey Hicks, Ph.D

Major Department: Chemistry

Alzheimer's disease (AD), an irreversible, progressive and devastating neurodegenerative disease, is the most common cause of dementia. It is characterized by the extracellular amyloid plaques and the intracellular neurofibrillary tangles. Amyloid plaques are majorly constituted of A $\beta$  peptides, which are cleaved from the membrane bound amyloid precursor protein (APP). A $\beta$  peptides consist of either 40 or 42 amino acid residues. Elevated concentrations of copper, zinc, and iron have been measured in amyloid plaques and recent in vitro studies have shown that zinc and copper ions promote the aggregation of these peptides. Furthermore, it was found that high affinity metal ion chelators can be used in the dissolution of aggregated A $\beta$  peptides. Taken together, these studies show the important role metal ions play in AD.

In vitro studies have shown that aggregation of human A $\beta$  peptides increases due to the presence of Cu, but this effect is much less profound for rat A $\beta$  peptides. Previous studies indicate that Cu<sup>2+</sup> binding occurs within the first 16 amino acid residues of the full length A $\beta$  peptides. Our lab has investigated the thermodynamics of Cu<sup>2+</sup> binding to A $\beta$ 16, A $\beta$ 28 and three

variant peptides using isothermal titration calorimetry (ITC) and ACES buffer as a weak competing ligand. In this study, the binding of  $\text{Cu}^{2+}$  to A $\beta$ 16 was studied at three different concentrations of ACES buffer (20mM, 50mM, and 100mM). Buffer independent binding constants (K) are then extracted to test for ternary complex formation. According to the thermodynamic studies of  $\text{Cu}^{2+}$  binding to A $\beta$ 28 and A $\beta$ 28 mutants, a model was proposed, which was further tested by obtaining the heat capacity ( $\Delta C_p$ ) data for  $\text{Cu}^{2+}$  binding to A $\beta$ 16 A $\beta$ 28 and A $\beta$ 28 mutants. In addition, heat capacity ( $\Delta C_p$ ) data for  $\text{Cu}^{2+}$  binding to Rat A $\beta$ 28 is obtained and compared to human A $\beta$ 28. Taken together, this data will be used to shed light on why the rat peptides do not form fibrils.

**Cu<sup>2+</sup> Binding to A $\beta$  peptides: Detailed Heat Capacity Studies Provide  
Structural Insight into Complex Formation**

A Thesis

Presented to

the Faculty of the Department of Chemistry

East Carolina University

Greenville, North Carolina

In Partial Fulfillment

of the Requirements for the Degree

Master's of Science in Chemistry

By:

Sunitha Gade

January, 2013

Copyright © 2013

**Cu<sup>2+</sup> Binding to A $\beta$  peptides: Detailed Heat Capacity Studies Provide  
Structural Insight into Complex Formation**

By Sunitha Gade

APPROVED BY:

DIRECTOR OF THESIS: \_\_\_\_\_

Anne M. Spuches, Ph.D.

COMMITTEE MEMBER: \_\_\_\_\_

John Kenney, Ph.D.

COMMITTEE MEMBER: \_\_\_\_\_

William E. Allen, Ph.D.

COMMITTEE MEMBER: \_\_\_\_\_

Colin Burns, Ph.D.

COMMITTEE MEMBER: \_\_\_\_\_

Allison S. Danell, Ph.D.

CHAIR OF THE DEPARTMENT OF CHEMISTRY: \_\_\_\_\_

Rickey P. Hicks, Ph.D.

DEAN OF THE GRADUATE SCHOOL: \_\_\_\_\_

Paul J. Gemperline, Ph.D.

## **Acknowledgments**

I would like to thank my advisor Dr. Anne Marie Spuches, Ph.D., for her guidance and support towards my research and thesis. I am grateful to her for valuable suggestions and commentary on everything I did and wrote in these years. I would also like to thank my thesis committee Dr. John Kenney, Dr. William E. Allen, Dr. Colin Burns, Dr. Allison S. Danell, for their valuable suggestions and support towards my research and in finalizing my thesis. I would like to specially thank my parents, my husband, my sister and brother-in-law, for their love, concern and support throughout my graduate studies.

# Table of Contents

Chapter 1: Introduction .....	1
1.1 Alzheimer's Disease .....	1
1.2 Hallmarks of Alzheimer's Disease .....	2
1.3 AD Pathogenesis.....	3
1.3.1 Amyloid Cascade Hypothesis (ACH).....	3
1.3.2 Metal Ion Hypothesis.....	5
1.3.3 Oxidative stress hypothesis.....	6
1.4 Binding of $\text{Cu}^{2+}$ to $\text{A}\beta$ .....	7
Chapter 2: Project Objectives and Design .....	10
2.1 Project Importance .....	10
2.2 Project Design .....	10
2.2.1 $\text{A}\beta$ Peptides .....	10
2.2.2 Buffer Considerations .....	11
2.3 Project Objectives .....	12
Chapter 3: Isothermal Titration Calorimetry (ITC) .....	17
3.1 Isothermal Titration Calorimetry .....	17
3.2 Thermodynamic Parameters .....	19
3.3 Fitting ITC Data.....	21
3.3.1 Single Set of Identical Sites .....	22
3.3.2 Two Sets of Independent Sites.....	23

3.3.3 Sequential Binding Sites .....	24
3.4 Thermodynamic Parameters .....	26
Chapter 4: Thermodynamic Results and Discussion .....	30
4.1 Materials .....	30
4.2 Sample Preparation .....	30
4.3 Isothermal Titration Calorimetry Conditions.....	31
4.4 Results and Discussion .....	32
4.4.1 Buffer Independent Studies.....	32
4.4.2 Temperature Dependence Studies: Cu <sup>2+</sup> Binding to Aβ28 and Mutant Peptides.....	34
4.4.2.1 Cu <sup>2+</sup> binding to Aβ28 .....	34
4.4.2.2 Cu <sup>2+</sup> binding to Aβ28H6A .....	38
4.4.2.3 Cu <sup>2+</sup> binding to Aβ28H13A .....	41
4.4.2.4 Cu <sup>2+</sup> binding to Aβ28H14A .....	44
4.4.3. Temperature Dependence Studies: Cu <sup>2+</sup> Binding to Rat Aβ28 .....	47
4.5 Temperature Dependence Studies: Discussion .....	51
4.6 Overall Conclusions.....	55
4.7 Future Studies .....	55

## List of Figures

<b>Figure 1.</b> Hallmarks of AD in Alzheimer's cells <sup>7</sup> .....	2
<b>Figure 2.</b> Amyloid Cascade Hypothesis <sup>5</sup> .....	4
<b>Figure 3.</b> Sequence of A $\beta$ peptide .....	4
<b>Figure 4.</b> A) Coordination sphere of Cu <sup>2+</sup> to A $\beta$ 16 (N-terminus, His6, His13 or His14, Asp1-COO <sup>-</sup> ). B) Coordination sphere B represents Cu <sup>2+</sup> to A $\beta$ 16 (His6, His13, His14, Asp1-COO <sup>-</sup> ). .....	9
<b>Figure 5.</b> Sequence of A $\beta$ peptide fragments. Red designates the specific substitutions in Rat peptide. ..	11
<b>Figure 6.</b> Sequence of A $\beta$ mutant peptides. Red designates the mutated residues.....	11
<b>Figure 7.</b> Structure of N-(2-Acetamido)-2-aminoethanesulfonic acid (ACES) .....	12
<b>Figure 8.</b> Cartoon representation of Cu <sup>2+</sup> bound to A) Human A $\beta$ 28 peptide and B) A $\beta$ 28 mutant peptides. ....	15
<b>Figure 9.</b> Sequence of human and rat A $\beta$ (40) peptide. Red and blue designates the three specific substitution residues .....	16
<b>Figure 10.</b> A typical isothermal titration calorimetry.....	17
<b>Figure 11.</b> Diagram shows the setup and the cell temperatures maintained in ITC.....	18
<b>Figure 12.</b> Diagram shows a typical raw and fitted data of ITC. ....	20
<b>Figure 13.</b> ITC integrated data representing the titration of Cu <sup>2+</sup> into A $\beta$ 16 with 20, 50, and 100 $\mu$ M ACES (pH=7.4). ....	32
<b>Figure 14.</b> Representative ITC data for the titration of 2.1 $\mu$ M Cu <sup>2+</sup> into 0.140 $\mu$ M A $\beta$ 28 at A) 10°C, B) 25°C, and C) 37°C.....	35
<b>Figure 15.</b> A plot of change in enthalpy verses temperature for the binding of 2.1 $\mu$ M Cu <sup>2+</sup> to A $\beta$ 28 for four sets is shown in the graph.....	37
<b>Figure 16.</b> Representative ITC data for the titration of 2.1 $\mu$ M Cu <sup>2+</sup> into 0.140 $\mu$ M A $\beta$ 28H6A at A) 10°C, B) 25°C, and C) 37°C.....	38

<b>Figure 17.</b> A plot of change in enthalpy verses temperature for the binding of 2.1 mM Cu <sup>2+</sup> to Aβ28H6A for three sets is shown.....	40
<b>Figure 18.</b> Representative ITC data for the titration of 2.1 mM Cu <sup>2+</sup> into 0.140 mM Aβ28H13A at A) 10°C, B) 25°C, and C) 37°C.....	41
<b>Figure 19.</b> A plot of change in enthalpy verses temperature for the binding of 2.1 mM Cu <sup>2+</sup> to Aβ28H13A for three sets is shown in the graph.....	43
<b>Figure 20.</b> Representative ITC data for the titration of 2.1 mM Cu <sup>2+</sup> into 0.140 mM Aβ28H14A at A) 10°C, B) 25°C, and C) 37°C.....	44
<b>Figure 21.</b> A plot of change in enthalpy verses temperature for the binding of 2.1 mM Cu <sup>2+</sup> to Aβ28H14A for three sets is shown in the graph.....	46
<b>Figure 22.</b> Representative ITC data for the titration of 2.1 mM Cu <sup>2+</sup> into 0.140 mM Rat Aβ28 at A) 10°C, B) 25°C, and C) 37°C.....	47
<b>Figure 23.</b> A plot of change in enthalpy verses temperature for the binding of 2.1 mM Cu <sup>2+</sup> to Rat Aβ28 for two sets is shown in the graph.....	50
<b>Figure 24.</b> Proposed Cu <sup>2+</sup> coordination for A) Human and B) Rat Aβ16 .....	52
<b>Figure 25.</b> Cartoon representation of Cu <sup>2+</sup> bound to A) Human Aβ28 peptide and B) Rat Aβ28 peptide. 53	
<b>Figure 26.</b> Parallel β-sheet A) Fibril formation in human Aβ28 peptide B) No fibril formation in Rat Aβ28 peptide.....	54

## List of Tables

<b>Table 1.</b> Concentrations of essential metals in normal brain and in amyloid plaques which are found in AD affected brains. ....	6
<b>Table 2.</b> Best fit ITC parameters and buffer dependant thermodynamic data collected previously. <sup>18</sup> .....	14
<b>Table 3.</b> Expected signs of $\Delta C_p$ and $\Delta S$ in protein reactions.....	29
<b>Table 4.</b> Buffer independent K and Kd values for A $\beta$ 16 peptide in 20mM, 50mM, and 100mM ACES (pH 7.4) with 100mM NaCl.....	33
<b>Table 5.</b> Best fit ITC parameters of Cu <sup>2+</sup> into A $\beta$ 28 at 10°C, 25°C, and 37°C.....	36
<b>Table 6.</b> Best fit ITC parameters of Cu <sup>2+</sup> into A $\beta$ 28H6A at 10°C, 25°C, and 37°C.....	39
<b>Table 7.</b> Best fit ITC parameters of Cu <sup>2+</sup> into A $\beta$ 28H13A at 10°C, 25°C, and 37°C.....	42
<b>Table 8.</b> Best fit ITC parameters of Cu <sup>2+</sup> into A $\beta$ 28H14A at 10°C, 25°C, and 37°C.....	45
<b>Table 9.</b> Best fit ITC parameters of Cu <sup>2+</sup> into Rat A $\beta$ 28 at 10°C, 25°C, and 37°C.....	49
<b>Table 10.</b> Heat capacity values for Cu <sup>2+</sup> binding to wild type, mutant type A $\beta$ 28 peptide and Rat A $\beta$ 28 peptide. Thermodynamic parameters values for Cu <sup>2+</sup> binding to peptides at 37°C.....	51

## Abbreviations

AD: Alzheimer's Disease

NFTs: Neurofibrillary Tangles

A $\beta$ : Amyloid Beta

ACH: Amyloid Cascade Hypothesis

APP : Amyloid Precursor Protein

Cu: Copper

Zn: Zinc

Fe: Iron

MT3: Metallothionein 3

CNS : Central Nervous System

ROS: Reactive Oxygen Species

Cu<sup>2+</sup>: Copper (II)

EPR: Electron Paramagnetic Resonance

CD: Circular Dichroism

ITC: Isothermal Titration Calorimetry

NMR: Nuclear Magnetic Resonance

FTIR : Fourier transform infrared spectroscopy

ESI-MS: Electrospray Ionization Mass Spectrometry

HPLC : High Performance Liquid Chromatography

HSAB: Hard Soft Acid Base Theory

N : Nitrogen

O : Oxygen

n: Stoichiometry

K: Binding Constant

$K_d$ : Dissociation Constant

$\Delta H$ : Change in Enthalpy

$\Delta S$ : Change in Entropy

$\Delta G$ : Gibbs Free Energy

$C_p$ : Heat Capacity at Constant Pressure

$\Delta C_p$ : Change in Heat Capacity

His : Histidine

Ala : Alanine

ACES: N-(2-Acetamido)-2-aminoethanesulfonic acid

CFB: Cell Feedback Network

## Chapter 1: Introduction

### 1.1 Alzheimer's Disease

Alzheimer's disease (AD) is an irreversible, progressive, and devastating neurodegenerative disease. It is the most common cause of dementia accounting for 60 to 80 percent of cases. The illness targets individuals 65 years of age and older, however 5 percent of individuals aged 40s or 50s are affected with early onset Alzheimer's.<sup>1</sup> Early onset Alzheimer's appears to be transmitted as a pure genetic, autosomal dominant trait.<sup>2</sup> It is currently estimated that AD is striking approximately 35 million victims worldwide, 5.4 million Americans and 170,000 North Carolinians. Currently, AD is the 6<sup>th</sup> leading cause of death in the United States.<sup>1</sup>

In AD's early stages, the most common symptom observed is short term memory loss. As the disease progresses, the symptoms include confusion, anger, language breakdown, mood swings, and long term memory loss. It is reported that people affected with AD live for an average of eight years after their symptoms become noticeable to others, but their survival can range from 4 to 20 years, depending on their age and other health conditions.<sup>1</sup> It is predicted that around 100 million people will be affected with AD by 2050. There is no current cure for AD, but there are treatments that temporarily delay the worsening of the symptoms.<sup>3</sup> The cause and progression of AD is still not known. Research progress indicates that AD is characterized by plaques and tangles.

## 1.2 Hallmarks of Alzheimer's Disease

In 1907, it was determined through biopsy that extracellular amyloid plaques and neurofibrillary tangles (NFT's) are the key pathological hallmarks of AD.<sup>4</sup> Figure 1 depicts amyloid plaques and NFT's in the AD affected brain. The amyloid plaques are caused by the aggregation of A $\beta$  peptides. They are dense deposits of cellular and protein material that aggregate around and outside of nerve cells. NFT's are the fibrillary aggregate of hyperphosphorylated tau protein, which build up in the cell body of the neuron and take its shape. NFT's consist of both paired helical and straight filaments of hyperphosphorylated tau,<sup>5</sup> a protein that stabilize microtubules. They are commonly observed upon neurodegeneration. Although the mechanism of senile plaques and neurofibrillary tangles is unclear, they are presumed to be responsible for neuronal death and loss of brain function.

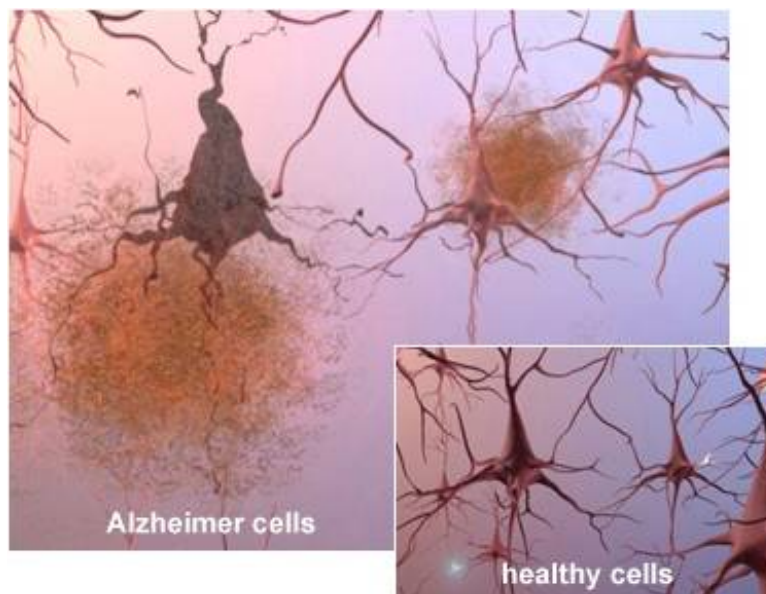


**Figure 1.** Hallmarks of AD in Alzheimer's cells.<sup>6</sup>

### 1.3 AD Pathogenesis

Focus on different features of AD has led to the development of three main hypotheses on the pathogenesis of AD: the amyloid cascade hypothesis, the metal ion hypothesis, and the oxidative stress hypothesis. Amyloid Cascade hypothesis states that imbalance between the A $\beta$  production and clearance is the pathogenic cause of AD and these amyloids are the main neurotoxic substances in AD. The metal ion hypothesis states that the impaired metal homeostasis, in particular of zinc (Zn), copper (Cu), and iron (Fe), with A $\beta$  imbalance being a consequence of this is the main cause of AD. The oxidative stress hypothesis states that the age enhanced or genetically and environmentally enhanced oxidative stress results in accumulated gene defects and declining mitochondrial function that subsequently leads to neurological disorders.<sup>7</sup>

#### 1.3.1 Amyloid Cascade Hypothesis (ACH)

ACH suggests that imbalance between the A $\beta$  production and clearance is the pathogenic cause of AD.<sup>8</sup> Figure 2 shows the ACH. The A $\beta$  peptide results from the enzymatic cleavage of amyloid precursor protein (APP) found in outer cell membrane and intracellularly in the membranes of organelles such as mitochondria. Studies have suggested two main pathways of the enzymatic cleavage of APP, the amyloidogenic and non-amyloidogenic. APP is a transmembrane protein that exists in different isoforms of 695-770 amino acids. In APP 695, A $\beta$  is located from amino acid 597-639. A $\beta$  consists of 39-43 amino acid residues. It has a large hydrophilic N-terminal domain (1-28) and a C-terminal hydrophobic domain (29-39/43).<sup>8</sup> APP is cleaved by  $\alpha$ -secretases at the  $\alpha$ -cleavage site led to the formation of sAPP  $\alpha$  peptides. In contrast  $\beta$ -secretases cleaved APP at  $\beta$ -site and then subsequent cleavage by  $\gamma$ -secretases led to the

formation of the two variants A $\beta$ 40 and A $\beta$ 42 peptides.<sup>9, 10</sup> Figure 3 includes the sequence of A $\beta$  peptide with both 40 and 42 amino acid residues.<sup>7</sup>

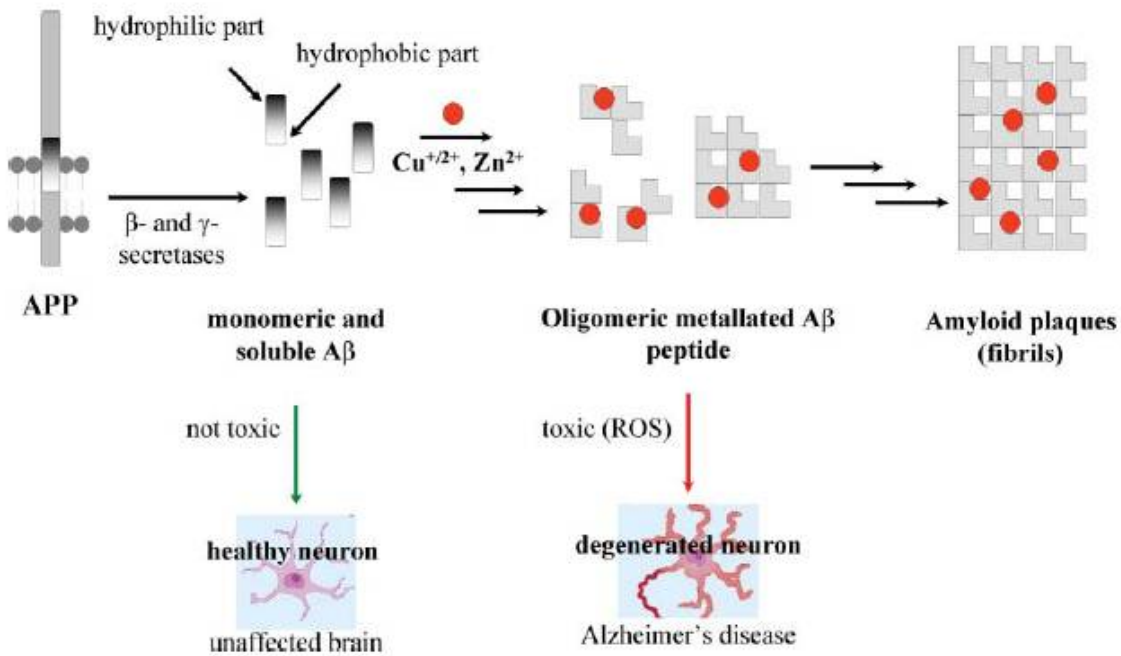


**Figure 2.** Amyloid Cascade Hypothesis<sup>8</sup>

DAEFRHDSGYEVHHQKLVFFAEDVGSNKGAIIGLMVGGVV<sub>40</sub>IA<sub>42</sub>

**Figure 3.** Sequence of A $\beta$  peptide

It has been described that A $\beta$  exists as three biochemical fractions in the brain: membrane associated, aggregated and soluble. The A $\beta$  peptides found in various forms react to produce soluble oligomers, which further tend to form protofibrils and ultimately to extracellular aggregates or fibrils which are the main constituent of the amyloid plaques.<sup>8</sup> It was found that in healthy individuals, most of the A $\beta$  is membrane associated, but in individuals with AD, most of the A $\beta$  is in the aggregated and soluble fraction which increases markedly.<sup>11</sup> Compared to the

soluble fraction there is an increase in the ratio of A $\beta$ 42/A $\beta$ 40 in amyloid plaques. A $\beta$ 42 is more toxic to neurons and more prone to aggregation than A $\beta$ 40.<sup>7</sup>

### 1.3.2 Metal Ion Hypothesis

Metal ion hypothesis states that transition metal ions, in particular of Cu, Zn and Fe, play an important role in the neuropathology of AD,<sup>12, 13</sup> However the exact mechanism is unknown.<sup>8,</sup><sup>14, 15</sup> The concentration of these metal ions in AD is significantly elevated and are listed accordingly in Table 1. Recent studies have shown that Zn and Cu are co-localized with the A $\beta$  deposits<sup>16</sup> and in vitro studies have suggested that these ions promote the A $\beta$  aggregation and toxicity, which lead to the development of AD.<sup>8, 14, 15</sup> Studies have reported the dissociation constant for the binding affinity of Cu and A $\beta$  range from attomolar to 11  $\mu$ M and for Zn and A $\beta$  range from 2-300  $\mu$ M.<sup>14</sup> Generally Cu and Zn are tightly bound to enzymes and other proteins and are released into the synaptic cleft during neurotransmission. Synaptic cleft region also consists of A $\beta$ , which has ability to interact with Zn and Cu and form amyloid. Metallothionein 3 (MT3), potent metal binding protein has ability to reduce the metal-A $\beta$  interactions, but their levels are decreased in AD.<sup>8, 15</sup>

**Table 1.** Concentrations of essential metals in normal brain and in amyloid plaques which are found in AD affected brains.<sup>8, 14, 15</sup>

	<b>Normal (<math>\mu\text{M}</math>)</b>	<b>Amyloid Plaques (<math>\mu\text{M}</math>)</b>
Copper	70	390
Zinc	350	1055
Iron	340	940

High concentrations of Fe ions are found in human amyloid plaques ( $\sim 1 \text{ mM}$ )<sup>8</sup>. In vivo studies have shown that Fe ion are not likely to interact with A $\beta$  and is not found in the co-purified extract of A $\beta$  from plaques.<sup>8</sup> Hence, the role of Fe ions in the neurodegenerative processes associated with AD will not be discussed as it does not interact directly with A $\beta$ .<sup>7</sup>

Zn plays a central role in the central nervous system (CNS). As mentioned previously, Zn is found in amyloid plaques and promotes A $\beta$  aggregation. Zn ion levels in amyloid plaques can be as high as  $\sim 1 \text{ mM}$ .<sup>8</sup> It is also reported that Zn is the only physiologically available metal ion to precipitate A $\beta$  at pH 7.4.<sup>11</sup> The A $\beta$ -Zn complex is reportedly more complicated. Hence, the role of Zn ions in the neurodegenerative processes associated with AD will not be discussed or studied.<sup>7</sup>

### **1.3.3 Oxidative stress hypothesis**

Oxidative stress hypothesis states an impaired oxidative stress response in the CNS leading to neurodegeneration. Oxidative stress results from the oxidative phosphorylation and most organisms have evolved to deal with the potential hazards of reactive oxygen species (ROS). Oxidative stress is also correlated with the mitochondrial function. Oxidative stress is found to be the primary cause of AD. However, oxidative stress can also be caused by the amyloid cascade. Toxic effects on mitochondria and amyloids in the toxic copper II ( $\text{Cu}^{2+}$ )

oligomer form are responsible for the generation of ROS. Hence, oxidative stress subsequently leads to neurological disorders.<sup>7</sup>

#### **1.4 Binding of Cu<sup>2+</sup> to A $\beta$**

Cu binding promotes the aggregation of A $\beta$ , it is important to know the coordination chemistry of Cu<sup>2+</sup> ions. Coordination of Cu<sup>2+</sup> with truncated peptides (A $\beta$ 16 and A $\beta$ 28) and full length peptides (A $\beta$ 40 and A $\beta$ 42) have been extensively studied in past few years. However, the identity of the coordination ligands is still unclear.<sup>8</sup>

Several studies have shown that two equivalents of Cu<sup>2+</sup> bind to A $\beta$  peptide in a sequential and ratiometric way by using different techniques like Electron Paramagnetic Resonance (EPR), Circular Dichroism (CD), Isothermal Titration Calorimetry (ITC). It is proposed that the first Cu<sup>2+</sup> equivalent has 100 times stronger affinity than second<sup>8</sup>. Other studies showed only one Cu<sup>2+</sup> binding site, because of the lower affinity of the second Cu<sup>2+</sup> equivalent.<sup>8, 15</sup>

According to hard/soft acid and base theory (HSAB) Cu shows affinity towards Nitrogen (N), and oxygen (O) ligands. Cu<sup>2+</sup> has a typical coordination number of 6 and can be smaller than 6, due to the strain imposed by the peptide backbone, the entropy release due to the chelate effect on binding a peptide chain, and the basicity of involved amino acid ligands. Hence, the coordination geometries of Cu<sup>2+</sup> are tetragonally distorted octahedral for coordination number 6 and trigonal bipyramidal for coordination number 5. Several studies indicate that the coordinating ligands with Cu<sup>2+</sup> are either three histidine (His) or two His residues and an N-terminal ligand. Several studies using nuclear magnetic resonance (NMR), Fourier transform infrared spectroscopy (FTIR), x-ray absorption spectroscopy, Electrospray Ionization Mass Spectrometry

(ESI-MS), sedimentation assay indicate the presence of all three His residues (His6, His13 and His14).<sup>6</sup> Potentiometric and EPR measurements have shown two types of Cu(A $\beta$ ) species at physiological pH (between pH6 and pH8).<sup>3</sup> The two types of Cu(A $\beta$ ) species are noted as species I (low pH) and species II (high pH). The transition between species I and species II has a midpoint at pH 8-8.7.<sup>8, 15</sup> EPR measurements showed that Cu<sup>2+</sup> coordination sphere at high pH consist of N atoms of His6, His13 and His14 and an O atom from the carboxylate group of Asp1 and only two His residues at low pH.<sup>6</sup>

Cu<sup>2+</sup> preferentially binds to ligands with low pK<sub>a</sub>. Hence, His (pK<sub>a</sub> - 6.5) and then N-terminus (pK<sub>a</sub> - 8) are preferred as the pK<sub>a</sub> of His is lower than N-terminus. N-terminus acetylation of A $\beta$ 16 and A $\beta$ 28 also showed profound changes in the speciation curve and CD signatures respectively. Hence, it was indirectly demonstrated that the Cu<sup>2+</sup> binding affinity was 3-4 times weaker in case of N-Acetylated Cu<sup>2+</sup>-A $\beta$  complex. Other studies showed the involvement of the His residues by considering mutated peptides. Studies showed modifications in the CD signatures of mutated peptides (His6Ala, His13Ala and His14Ala) compared to non-mutated peptides. Finally, it was concluded that the N ligands of the Cu<sup>2+</sup> ion are the three His residues or the two His residues and the N-terminus. Recent studies proposed models of the two most likely coordination spheres of Cu<sup>2+</sup> to A $\beta$  peptide at physiological pH. As shown in Figure 4 coordination sphere **A** represents Cu<sup>2+</sup> to A $\beta$  (N-terminus, His6, His13 or His14, Asp1-COO<sup>-</sup>) and coordination sphere **B** represents Cu<sup>2+</sup> to A $\beta$  (His6, His13, His14, Asp1-COO<sup>-</sup>).<sup>3</sup>

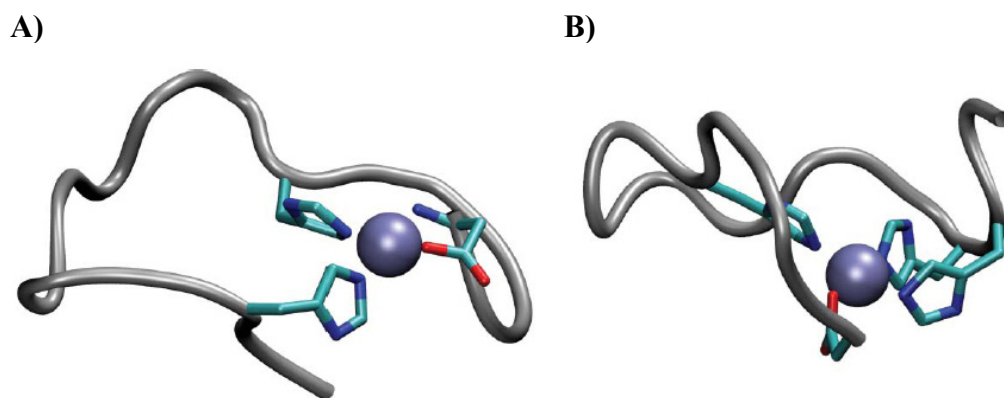


**Figure 4.** A) Coordination sphere of Cu<sup>2+</sup> to Aβ16 (N-terminus, His6, His13 or His14, Asp1-COO<sup>-</sup>). B) Coordination sphere B represents Cu<sup>2+</sup> to Aβ16 (His6, His13, His14, Asp1-COO<sup>-</sup>).<sup>8</sup>

## **Chapter 2: Project Objectives and Design**

### **2.1 Project Importance**

The purpose of this research is to provide insight into the role played by  $\text{Cu}^{2+}$  ions in amyloid plaque formation and its affinity towards human  $\text{A}\beta$  peptides and rat  $\text{A}\beta$  peptides. ITC is a powerful technique used to obtain the thermodynamic profile of metals binding to  $\text{A}\beta$ -peptides. The binding constant (K), change in enthalpy ( $\Delta\text{H}$ ), change in entropy ( $\Delta\text{S}$ ), and Gibbs free energy ( $\Delta\text{G}$ ) are obtained using ITC. The binding constant reflects the stability of the metal and protein complex while the  $\Delta\text{H}$ ,  $\Delta\text{S}$ , and change in heat capacity ( $\Delta\text{C}_p$ ) data indirectly provides us with conformational changes in protein upon metal binding. All this information allows us to build a model of metal binding to these peptides. Thermodynamic data collected in Spuches lab aided for the proposal of models for  $\text{Cu}^{2+}$  binding to  $\text{A}\beta_{16}$ ,  $\text{A}\beta_{28}$ , and  $\text{A}\beta_{28}$  mutants.<sup>17</sup> The thermodynamic data may also aid the development of more useful metal chelators for drug therapy.

### **2.2 Project Design**

#### **2.2.1 $\text{A}\beta$ Peptides**

Studies have proposed that the metal binding site lies within the first 16 amino acids ( $\text{A}\beta_{16}$ ) of  $\text{A}\beta$ .  $\text{A}\beta_{16}$  is considered a decent model because it does not tend to aggregate or to form fibrils under moderate conditions. Another truncated  $\text{A}\beta$  peptide with amino acids 1-28 ( $\text{A}\beta_{28}$ ) has been studied though it aggregates and forms fibrils under moderate conditions at slower rate than full length  $\text{A}\beta$  peptide ( $\text{A}\beta_{40}$  or  $\text{A}\beta_{42}$ ). Rat  $\text{A}\beta_{28}$  peptide has also been studied.  $\text{A}\beta$  peptide sequences studied are as shown in Figure 5.

Human A $\beta$ 16 DAEFRHDSGYEVHHQK<sub>16</sub>  
 Human A $\beta$ 28 DAEFRHDSGYEVHHQKLVFFAEDVGSNK<sub>28</sub>  
 Rat A $\beta$ 28 DAEFGHDSGFEV<sup>R</sup>HQKLVFFAEDVGSNK<sub>28</sub>

**Figure 5.** Sequence of A $\beta$  peptide fragments. Red designates the specific substitutions in Rat peptide.

In addition to these peptides, mutated A $\beta$ 28 peptides have also been studied. His residues at positions 6, 13 and 14 were mutated with alanine (Ala) residues. Previously in Spuches lab the thermodynamic parameters of Cu<sup>2+</sup> binding to A $\beta$ 16, A $\beta$ 28, and A $\beta$ 28 mutant peptides have been studied. A $\beta$ 28 mutant peptides were studied to know the involvement of the histidine residues in the coordination spheres. The mutated A $\beta$ 28 peptides studied are shown in the Figure 6.<sup>17</sup>

A $\beta$ 28 (H6A) DAEFR<sup>A</sup>DSGYEVHHQKLVFFAEDVGSNK  
 A $\beta$ 28 (H13A) DAEFRHDSGYEV<sup>A</sup>HQKLVFFAEDVGSNK  
 A $\beta$ 28 (H14A) DAEFRHDSGYEVH<sup>A</sup>QKLVFFAEDVGSNK

**Figure 6.** Sequence of A $\beta$  mutant peptides. Red designates the mutated residues.

### 2.2.2 Buffer Considerations

In our studies, we use the buffer as a chelator for two reasons. It is used to keep the metal from precipitating and to allow us to accurately measure the binding constant. It is also important to choose a buffer which acts as a weak chelator. Therefore, in this case we used N-(2-Acetamido)-2-aminoethanesulfonic acid (ACES) as a buffer. ACES is considered as it acts as a

weak chelator for copper. The affinity of ACES for Cu is also known (Log  $K_{MB}$ =4.32 and Log  $K_{MB_2}$ =7.77). In metal solution chemistry, it is important to consider metal buffer interactions. Therefore, buffer independent binding constants should be calculated, which is further discussed in the next sections. This information provided helps in choosing ACES as a weak chelating buffer. Figure 7 shows the structure of N-(2-Acetamido)-2-aminoethanesulfonic acid (ACES).

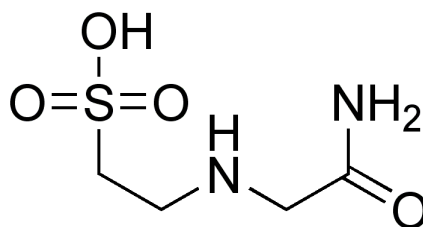


**Figure 7.** Structure of N-(2-Acetamido)-2-aminoethanesulfonic acid (ACES)

### 2.3 Project Objectives

In metal solution chemistry, it is important to consider metal-buffer interactions. Buffer-independent binding constant ( $K$ ) and dissociation constant ( $K_d$ ) were extracted using recently developed methods.<sup>17 18</sup> The equation used to extract buffer-independent binding constant ( $K$ ) is listed below.

$$K_{M-Peptide} = K_{ITC} \left( 1 + K_{MB} [B] + K_{MB_2} [B]^2 \right) \quad \text{Eq. 1}^{17}$$

In our present study ACES is used as a buffer and a weak chelator for  $\text{Cu}^{2+}$ .  $\text{Cu}^{2+}$  is titrated with A $\beta$ -16 in 20 mM ACES buffer (pH=7.4) and 100 mM NaCl at 37 °C.

Thermodynamic parameters obtained from fitting ITC data are listed in Table 2. From the obtained condition dependent constants, we can extract  $K$  and  $K_d$ . Upon substituting the obtained  $K_{ITC}$  value,  $K_{MB}$ ,  $K_{MB_2}$ , and concentration of buffer  $[B]$  into the above equation 1, the  $K$  of  $1.1 (\pm 0.13) \times 10^9 \text{ M}^{-1}$  and  $K_d$  of  $0.95 (\pm 0.1) \text{ nM}^{17}$  was obtained. Buffer independent  $K$  values obtained using ACES as a competing ligand are comparable to those reported by Hatcher et al, with an association constant that is smaller by a factor of 3.<sup>19</sup>

One criticism of using small molecules as competing chelators for  $\text{Cu}^{2+}$  is the formation of ternary complexes between the metal, peptide and small molecule.<sup>15, 20, 21</sup> One aim of this research was to determine if there is potential formation of ternary complexes. Therefore, titration of  $\text{Cu}^{2+}$  into A $\beta$ 16 is performed at two additional buffer concentrations. If the buffer independent values are similar at different concentrations, then we can suggest that ternary complex formation is insignificant.

Previously in the Spuches lab, thermodynamic parameters for  $\text{Cu}^{2+}$  binding to A $\beta$ 28 and A $\beta$ 28 mutant peptides were obtained using ITC.<sup>17</sup> According to the data, the  $\Delta G$  is similar for both wild and mutant type A $\beta$ 28 peptide. However, there is a decrease in copper binding enthalpy by approximately 1 kcal/mol for each mutant. This decrease is compensated by increase in T $\Delta S$  of approximately 1 kcal/mol for each mutant.

**Table 2.** Best fit ITC parameters and buffer dependant thermodynamic data collected previously.<sup>17</sup>

Peptide	N	K ( $\times 10^4$ )	$\Delta G$ (kcal/mol)	$\Delta H$ (kcal/mol)	T $\Delta S$ (kcal/mol)
A $\beta$ 16	1.00 ( $\pm 0.02$ )	7.6 ( $\pm 0.9$ )	-6.9 ( $\pm 0.1$ )	-2.7 ( $\pm 0.1$ )	4.2 ( $\pm 0.1$ )
A $\beta$ 28	1.02 ( $\pm 0.06$ )	4.2 ( $\pm 0.7$ )	-6.5 ( $\pm 0.1$ )	-3.2 ( $\pm 0.2$ )	3.3 ( $\pm 0.2$ )
A $\beta$ 28 (H6A)	0.92 ( $\pm 0.05$ )	3.3 ( $\pm 0.8$ )	-6.4 ( $\pm 0.1$ )	-2.2 ( $\pm 0.1$ )	4.3 ( $\pm 0.1$ )
A $\beta$ 28 (H13A)	0.85 ( $\pm 0.04$ )	5.7 ( $\pm 1.6$ )	-6.7 ( $\pm 0.2$ )	-2.0 ( $\pm 0.1$ )	4.7 ( $\pm 0.2$ )
A $\beta$ 28 (H14A)	0.95 ( $\pm 0.03$ )	4.8 ( $\pm 1.0$ )	-6.6 ( $\pm 0.1$ )	-2.3 ( $\pm 0.1$ )	4.3 ( $\pm 0.2$ )

Two models were proposed to explain the observed changes in entropy upon Cu<sup>2+</sup> binding to mutant A $\beta$ 28 peptides.<sup>12</sup>

**Model 1:** According to Model 1, there may be a shift in equilibrium that favors the formation of fewer species in solution. This means less conformational restriction in the peptide backbone upon Cu<sup>2+</sup> binding, which would result in more favorable entropy.

**Model 2:** According to Model 2, they may form more compact structures in solution with less exposed hydrophobic residues. This may result in the release of ordered water molecules into the bulk solvent and an increase in the entropy of the system.

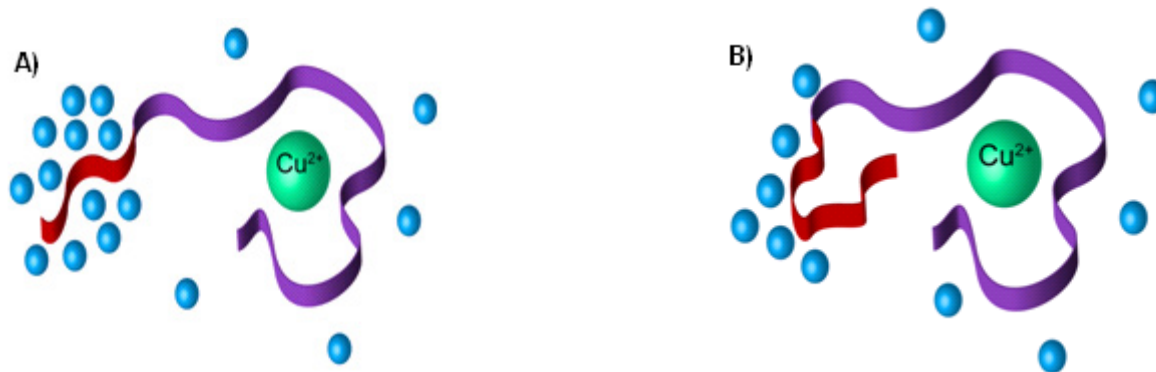


**Figure 8.** Cartoon representation of  $\text{Cu}^{2+}$  bound to A) Human  $\text{A}\beta_{28}$  peptide and B)  $\text{A}\beta_{28}$  mutant peptides. Red patch represents a hydrophobic patch in both the peptides. Blue balls represent water molecules. Each cartoon represents an “average”  $\text{Cu}^{2+}$ -peptide structure in solution and highlights the ordered water molecules surrounding the hydrophobic residues. The figure was generated with Adobe Illustrator CS4.<sup>17</sup>

Our second aim was to further test the second model. Heat capacity ( $C_p$ ) of a substance is the amount of heat required to change its temperature by one degree unit. The more ways the heat energy is distributed in a substance, the higher the heat capacity. The  $\Delta H$  and  $\Delta S$  of any object are integral functions of its heat capacity.<sup>22</sup> The  $\Delta C_p$  is generally observed to be positive when a protein unfolds, while a negative  $\Delta C_p$  is observed upon protein folding.<sup>23-26</sup> Heat capacity studies will be performed to test Model 2 by titrating  $\text{Cu}^{2+}$  into  $\text{A}\beta$  peptides at different temperatures (10 °C, 25 °C and 37 °C). If the mutant peptides do form more compact structures with less exposed hydrophobic residues upon  $\text{Cu}^{2+}$  binding, then one would observe a less positive  $\Delta C_p$  for the  $\text{A}\beta_{28}$  mutants than wild-type  $\text{A}\beta_{28}$ . This result would support Model 2.

$$\Delta C_p = \Delta H / \Delta T$$

**Eq. 2<sup>24</sup>**

A third aim of this research is to study  $\text{Cu}^{2+}$  binding to Rat A $\beta$  peptides. Rats rarely form amyloid plaques with age.<sup>27</sup> In vitro studies showed that aggregation of human A $\beta$  peptides increases due to the presence of Cu, but this effect is much less profound for rat A $\beta$  peptides. The difference between human and rat A $\beta$  peptide is the presence of three specific substitutions in the primary amino acid sequence: R5G, Y10F, and H13R, as shown in Figure 9.<sup>27</sup> All three mutations lie within the hydrophilic N-terminal, which is also the domain where  $\text{Cu}^{2+}$  binds.<sup>27</sup>

Human A $\beta$ (40)    DAEFRHDSG**Y**EV**H**HQKLVFFAEDVGSNKGAIIGLMVGGVV  
Rat A $\beta$ (40)        DAEF**G**HDSG**F**EV**R**HQKLVFFAEDVGSNKGAIIGLMVGGVV

**Figure 9.** Sequence of human and rat A $\beta$ (40) peptide. Red and blue designates the three specific substitution residues.

ITC was used to measure the thermodynamic parameters of Rat A $\beta$ 28 peptide and heat capacity studies were performed to investigate the difference between  $\text{Cu}^{2+}$  binding to human and rat A $\beta$  peptides.

## Chapter 3: Isothermal Titration Calorimetry (ITC)

### 3.1 Isothermal Titration Calorimetry (ITC)

ITC is a quantitative technique used to determine the thermodynamic parameters of biomolecular interactions in solution. It is most often used to study the interactions between ligand/metal and macromolecule/protein. ITC measures the heat absorbed or released during the biomolecular interactions.<sup>28</sup> The thermodynamic data provided includes stoichiometry ( $n$ ),  $K$ ,  $\Delta H$  and  $\Delta S$ .

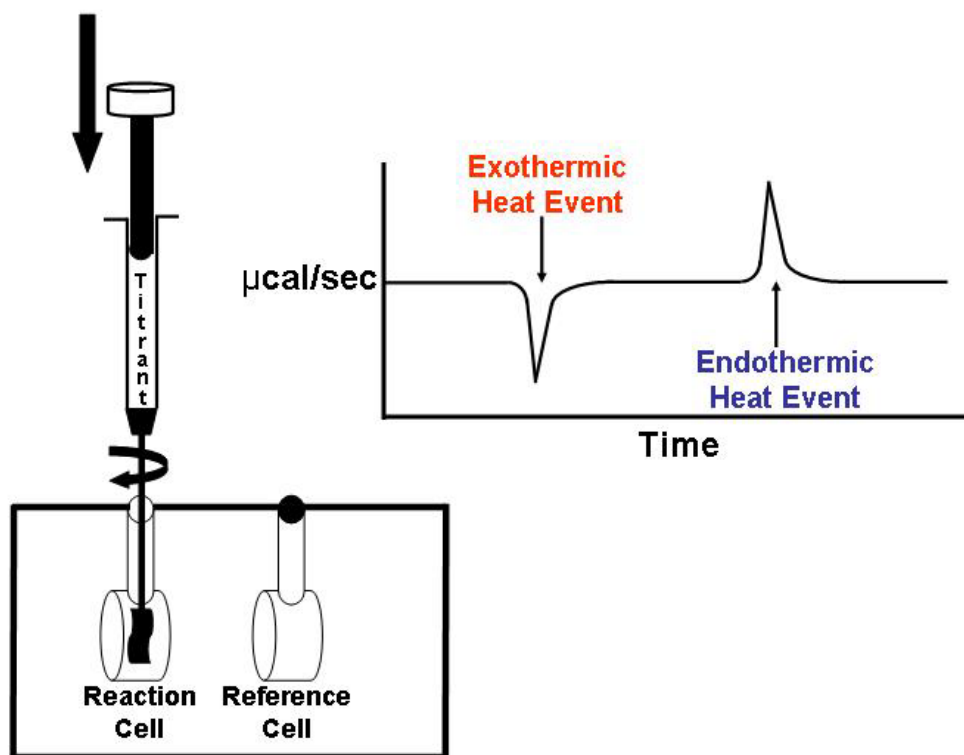


**Figure 10.** A typical isothermal titration calorimetry<sup>29</sup>

Figure 10 illustrates a typical ITC setup. The instrument consists of two identical cells, the reaction cell and the reference cell, contained in an adiabatic jacket and maintained at

identical temperatures. During the experiment, an automated syringe is placed into the reaction cell to deliver the titrant (ligand/metal) solution and ensure mixing.

In a typical ITC experiment, the reaction cell is filled with the protein solution and the syringe is filled with the titrant (ligand/metal) solution. During the experiment, the titrant is introduced into the reaction cell in known aliquots. Binding results in either heat loss or gain. If heat is released during the reaction, a negative peak corresponding to the exothermic event is observed. Alternatively, if the heat is absorbed during the reaction, a positive peak corresponding to the endothermic event is observed (Figure 10). Each peak observed is representative of a reaction that has gone to equilibrium.

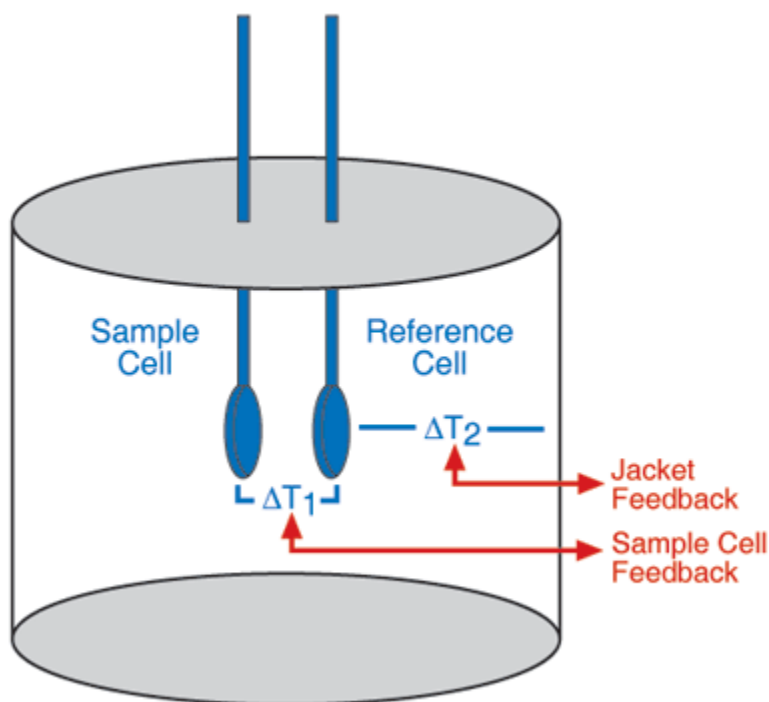


**Figure 11.** Diagram shows the setup and the cell temperatures maintained in ITC.

ITC utilizes a cell feedback network (CFB) mechanism during operation.<sup>28</sup> The calorimeter consists of a thermoelectric device which measures the temperature difference between the reaction cell and the reference cell referred to as  $\Delta T_1$ . Another thermoelectric device is used to measure the temperature difference between the jacket and the cells referred to as  $\Delta T_2$ .  $\Delta T_1$  and  $\Delta T_2$  are shown in Figure 11. Heat absorbed or released during a reaction is reflected in the temperature difference between the reaction and reference cell ( $\Delta T_1$ ) and is compensated by the addition or removal of the heat, as appropriate, using the CFB system.<sup>28</sup>

### **3.2 Thermodynamic Parameters**

ITC provides a complete thermodynamic profile of biomolecular interactions in a single experiment. Figure 12 is an ideal data set illustrating an exothermic reaction. The raw data ( $\mu\text{cal}/\text{sec}$ ) is integrated to obtain the binding isotherm ( $\text{kcal}/\text{mol}$  of injectant), as shown in Figure 12. This data is then fit to a model (discussed below) to obtain the  $n$ ,  $K$  and  $\Delta H$  as shown in the Figure 12.<sup>29</sup>

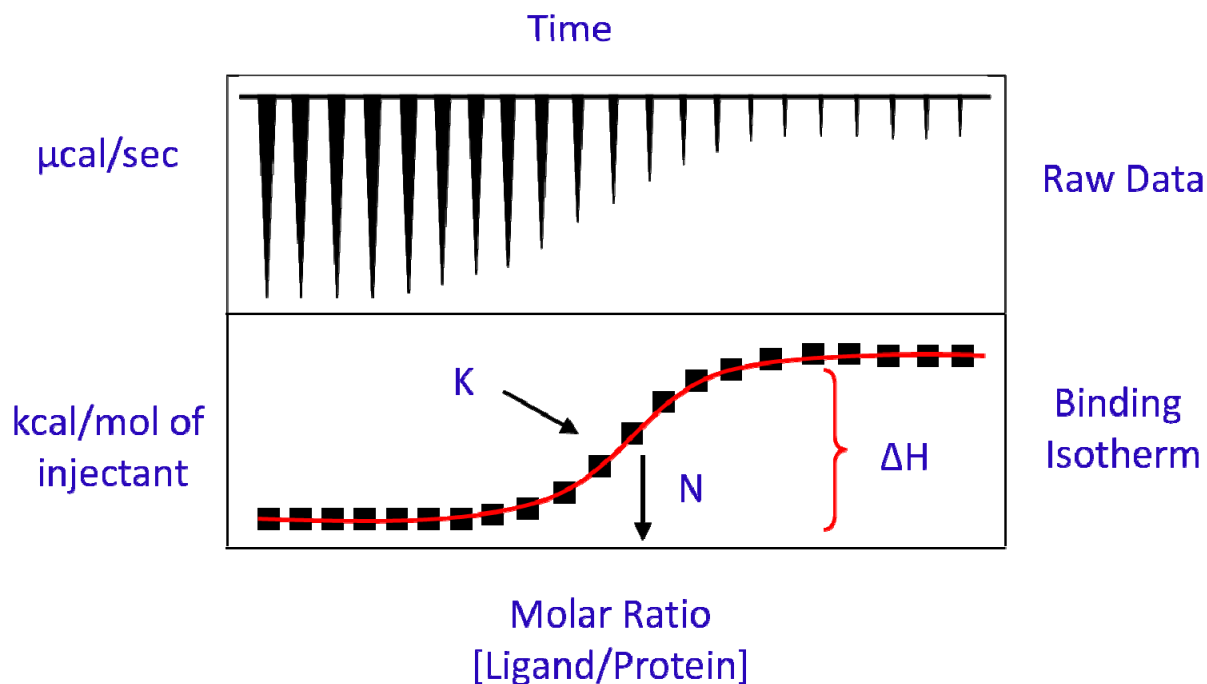


**Figure 12.** Diagram shows a typical raw and fitted data of ITC.<sup>29</sup>

As shown in Figure 12, the inflection point of the binding isotherm represents the  $n$  which discloses the metal to protein ratio. The slope of the binding isotherm provides us with the  $K$ , which represents the strength of binding. A steep slope indicates strong binding and a shallow slope indicates weak binding. The  $K$  is determined using an equilibrium expression (Eq. 3), where  $M$  denotes the macromolecule and  $X$  denotes the ligand. The  $\Delta H$  is obtained as the difference of the heat of reaction and heat of dilution.<sup>30</sup>

$$K = \frac{[MX]}{[M][X]}$$

Eq. 3<sup>30</sup>

The obtained three parameters (n, K,  $\Delta H$ ) are used to calculate the other thermodynamic parameters ( $\Delta G$ ,  $\Delta S$ ).  $\Delta G$  can be calculated using the Eq. 4, where R indicates the ideal gas constant, T indicates the temperature, which is held constant throughout the experiment, K indicates the binding constant obtained from the slope of the binding isotherm.

$$\Delta G = -RT \ln K \quad \text{Eq. 4}^{30}$$

$\Delta S$  can be calculated using the Eq. 5, where  $\Delta G$  indicates the change in the Gibbs free energy,  $\Delta H$  indicates the change in enthalpy of the reaction and  $T\Delta S$  is the change in the entropy at experimental temperature.

$$\Delta G = \Delta H - T\Delta S \quad \text{Eq. 5}^{30}$$

### 3.3 Fitting ITC Data

ITC data is fitted using Origin<sup>®</sup> software, version 7.0. This software includes three common fitting models that are applicable to wide range of binding phenomenon. The three common fitting models include single set of identical sites, two sets of independent sites, and sequential binding sites models.<sup>30</sup>

In general, the process of fitting data includes four steps 1) initial guesses (which most often can be made accurately enough by origin) of n, K, and  $\Delta H$ ; 2) calculation of  $\Delta Q(i)$  for each injection and comparison of these values with the measured heat for the corresponding experimental injection; 3) improvement in the initial values of n, K, and  $\Delta H$  by standard

Marquardt methods; 4) iteration of the above procedure until no further significant improvement in fit occurs with continued iteration.<sup>30</sup>

### 3.3.1 Single Set of Identical Sites

This model is used to fit the data for the molecule with a single set of binding sites. The  $K$  that describes ligand binding to macromolecule is given by the Eq. 6, where  $K$  is the binding constant,  $[X]$  is the free concentration of ligand, and  $\Theta$  is the fraction of sites occupied by ligand  $X$ .<sup>30</sup>

$$K = \frac{\Theta}{(1-\Theta)[X]} \quad \text{Eq. 6}^{30}$$

The bulk concentration of the ligand,  $X_t$ , is given by the Eq. 7, where  $[X]$  is the free concentration of ligand,  $n$  is the number of sites,  $\Theta$  is the fraction of sites occupied by ligand  $X$ , and  $M_t$  is the bulk concentration of macromolecule in  $V_o$ .<sup>30</sup>

$$X_t = [X] + n\Theta M_t \quad \text{Eq. 7}^{30}$$

Combining Eqs. 6 and 7 gives Eq. 8 below.

$$\Theta^2 - \Theta \left[ 1 + \frac{X_t}{nM_t} + \frac{1}{nKM_t} \right] + \frac{X_t}{nM_t} = 0 \quad \text{Eq. 8}^{30}$$

The total heat content  $Q$  of the solution contained in  $V_o$  at fractional saturation  $\Theta$  is given by Eq. 9, where  $\Delta H$  is the molar heat of ligand binding, and  $V_o$  is the active cell volume.

$$Q = n\Theta M_t \Delta H V_o \quad \text{Eq. 9}^{30}$$

The heat content  $Q$  value can be calculated at the end of the  $i^{\text{th}}$  injection and can be designated as  $Q(i)$ . Solving the quadratic Eq. 8 for  $\Theta$  and then substituting this into Eq. 9 gives  $Q(i)$  (Eq. 10).

$$Q_{(i)} = \frac{nM_t \Delta H V_o}{2} \left[ 1 + \frac{X_t}{nM_t} + \frac{1}{nKM_t} - \sqrt{\left(1 + \frac{X_t}{nM_t} + \frac{1}{nKM_t}\right)^2 - \frac{4X_t}{nM_t}} \right] \quad \text{Eq. 10}^{30}$$

### 3.3.2 Two Sets of Independent Sites

The two sets of independent sites model is similar to the above model except for the addition of second set of sites. The binding constants  $K_1$  and  $K_2$  were given by the Eq. 11.<sup>30</sup>

$$K_1 = \frac{\Theta_1}{(1-\Theta_1)[X]} \quad \text{Eq. 11}^{30}$$

$$K_2 = \frac{\Theta_2}{(1-\Theta_2)[X]}$$

Solving the Eq. 11 for  $\Theta_1$  and  $\Theta_2$  independently is given as shown in the Eq. 12

$$\Theta_1 = \frac{M_t [X] K_1}{1 + [X] K_1} \quad \text{Eq. 12}^{30}$$

$$\Theta_2 = \frac{M_t[X]K_2}{1 + [X]K_2}$$

As shown in the above model bulk concentration of ligand can be calculated using Eq. 13

$$X_t = [X] + M_t(n_1\Theta_1 + n_2\Theta_2) \quad \text{Eq. 13}^{30}$$

Substituting Eq. 12 into Eq. 13 gives Eq. 14.

$$X_t = [X] + M_t \left( \frac{n_1\Delta H_1 M_t [X] K_1}{1 + [X] K_1} + \frac{n_2\Delta H_2 M_t [X] K_2}{1 + [X] K_2} \right) \quad \text{Eq. 14}^{30}$$

As mentioned in the previous model, the heat content after any injection,  $i$ , is given according to the Eq. 15.

$$Q_{(i)} = M_t V_o (n_1 \Delta H_1 \Theta_1 + n_2 \Delta H_2 \Theta_2) \quad \text{Eq. 15}^{30}$$

By substituting the  $\Theta_1$  and  $\Theta_2$  in Eq. 15 gives Eq. 16

$$Q_{(i)} = M_t V_o \left( \frac{n_1 \Delta H_1 M_t [X] K_1}{1 + [X] K_1} + \frac{n_2 \Delta H_2 M_t [X] K_2}{1 + [X] K_2} \right) \quad \text{Eq. 16}^{30}$$

### 3.3.3 Sequential Binding Sites

For sequential binding, the binding constants  $K_1, K_2, K_3, \dots$  are given relative to the progress of saturation.<sup>30</sup>

$$K_1 = \frac{[MX]}{[M][X]} \quad K_2 = \frac{[MX_2]}{[MX][X]} \quad K_3 = \frac{[MX_3]}{[MX_2][X]} \quad \text{Eq. 17}^{30}$$

This means that there is no difference as to which sites are saturated, but only the total number of sites saturated can be determined. The concentration of all ligated species  $[ML_i]$  can be expressed in terms of the concentration of the non-ligated species  $[M]$ . The fraction of macromolecule  $F_i$ , having  $i$  bound ligands can be determined.<sup>30</sup>

$$F_0 = \frac{1}{1 + K_1[X] + K_1K_2[X]^2 + K_1K_2K_3[X]^3} \quad \text{Eq. 18}^{30}$$

$$F_1 = \frac{K_1[X]}{1 + K_1[X] + K_1K_2[X]^2 + K_1K_2K_3[X]^3} \quad \text{Eq. 19}^{30}$$

$$F_2 = \frac{K_1K_2[X]^2}{1 + K_1[X] + K_1K_2[X]^2 + K_1K_2K_3[X]^3} \quad \text{Eq. 20}^{30}$$

$$F_3 = \frac{K_1K_2K_3[X]^3}{1 + K_1[X] + K_1K_2[X]^2 + K_1K_2K_3[X]^3} \quad \text{Eq. 21}^{30}$$

The bulk concentration of the ligand  $X_t$  can be expressed in terms of  $[X]$  and  $M_t$ , given by the Eq. 22.

$$X_t = [X] + M_t \sum_{i=1}^n iF_i \quad \text{Eq. 22}^{30}$$

Once  $n$  and fitting parameters  $K_1$  through  $K_n$  are assigned, then Eqs. 18 - 21 can be used to calculate the free concentration of the ligand  $[X]$  by numerical methods (Bisection method). Once  $[X]$  is calculated, all  $F_i$  can be calculated from Eq. 19. The heat content  $Q$  after the  $i^{\text{th}}$  injection is calculated by the given Eq. 23.<sup>30</sup>

$$Q = M_t V_o (F_1 \Delta H_1 + F_2 [\Delta H_1 + \Delta H_2] + F_3 [\Delta H_1 + \Delta H_2 + \Delta H_3]) \quad \text{Eq. 23}^{30}$$

All these fitting models evaluate the change in the heat content,  $\Delta Q(i)$ , from the completion of the  $i-1$  injection to completion of the  $i$  injection. The change in the heat content,  $\Delta Q(i)$ , is given by the Eq. 24, where  $V_o$  is the active cell volume,  $V_i$  is the volume of the  $i^{\text{th}}$  injection, and  $Q(i)$  is the heat from the  $i^{\text{th}}$  injection.<sup>30</sup>

$$\Delta Q(i) = Q(i) + \frac{dV_i}{V_o} \left[ \frac{Q(i) + Q(i-1)}{2} \right] - Q(i-1) \quad \text{Eq. 24}^{30}$$

### 3.4 Thermodynamic Parameters

The thermodynamic parameters  $n$ ,  $K$ ,  $\Delta H$ ,  $\Delta S$ , and  $\Delta G$  were obtained using ITC. These parameters provide information regarding the interactions in solution. In addition,  $\Delta C_p$  may also be obtained from ITC data. All the thermodynamic parameters will be further discussed below.

The equilibrium reaction for the binding of a metal to a peptide is represented by Eq. 25. An equilibrium expression can be obtained for this reaction and is represented by Eq. 26 where  $K$  is the equilibrium or more specifically binding constant. If the resulting  $K$  value is much greater than one, the reaction lies towards the production of products while a  $K$  less than one

indicates that the reaction favors reactants. Thus, large K values indicate a tight binding interaction while small K values indicate weak binding interactions.



$$K = \frac{[\text{Metal - Peptide}]}{[\text{Metal}][\text{Peptide}]} \quad \text{Eq. 26}$$

$\Delta G$  predicts the spontaneity of the reaction at constant temperature and pressure. It accounts for the difference in energy between bound and unbound states. A negative  $\Delta G$  value indicates a favorable chemical reaction. It also describes that the progress of the reaction requires no energy input into the system. A positive  $\Delta G$  value indicates an unfavorable chemical reaction. It also describes that the progress of the reaction requires input of energy from the surroundings into the system.  $\Delta G$  with a negative value is termed as exergonic and  $\Delta G$  with a positive value is termed as endergonic. The  $\Delta G$  is a function of K according to Eq. 4 and is a function of  $\Delta H$ , and  $\Delta S$  according to Eq. 5.

$\Delta H$  indicates the heat of the reaction resulting from bond formation or bond breakage. In a reaction, if heat is released it indicates that there is an exothermic heat event which results in a negative  $\Delta H$ . A negative  $\Delta H$  is indicative of more favorable bonding interactions (van der Waals, ionic, covalent, and H-Bonding). If heat is absorbed from the surroundings it indicates that there is an endothermic heat event which results in a positive  $\Delta H$ . A positive  $\Delta H$  suggests weaker interactions or the disruption of these interactions.

$\Delta S$  is defined as the measure of the dispersion of energy within the system. Positive  $\Delta S$  relates back to the number of ways you can disperse energy in your system. It relates to

conformational degrees of freedom within your molecule and also solvation effects. Therefore a positive  $\Delta S$  value indicates a favorable chemical reaction and a negative  $\Delta S$  value indicates an unfavorable chemical reaction.  $\Delta S$  is obtained as the ratio of the heat absorbed to the absolute temperature, as given in Eq. 27.

$$\Delta S = \frac{q}{T} \quad \text{Eq. 26}$$

$\Delta C_p$  is a measure of the capacity of any object to take up heat energy.  $\Delta C_p$  can be calculated as shown in Eq. 2. The more ways there are of distributing heat energy in a substance, the higher will be its heat capacity.<sup>22</sup> The major sources responsible for  $\Delta C_p$  and  $\Delta S$  are the hydrophobic effect, conformational entropy, and intramolecular vibrations. Expected signs of  $\Delta C_p$  and  $\Delta S$  in protein reactions are indicated as shown in the table 3.<sup>24</sup>

$$\Delta C_p = \frac{\Delta H}{\Delta T} \quad \text{Eq. 2}$$

**Table 3.** Expected signs of  $\Delta C_p$  and  $\Delta S$  in protein reactions.<sup>24</sup>

<b>For an increase in the following:</b>	<b><math>\Delta C_p</math></b>	<b><math>\Delta S</math></b>
exposure of nonpolar groups	+	-
exposure of electrostatic charges	-	-
hydrogen bonds	+	-
conformations (isoenergetic)	0	+
soft internal modes	+	+

Conformational entropy is the entropy associated with the isoenergetic conformations available to a protein. An increase in the number of isoenergetic conformations results in an increase in its entropy but does not affect the heat capacity to a great extent. Intramolecular vibrations are characterized by the internal degrees of freedom or internal vibrational modes. The hydrophobic effect is the tendency of the non-polar groups to aggregate in aqueous solution and exclude water molecules. This effect results in the formation of clathrates or structured water around non-polar groups, which in turn results in an increase in the heat capacity of solutes.<sup>24</sup> In regards to protein folding (as mentioned in chapter 2) positive  $\Delta C_p$  indicates protein unfolding and negative  $\Delta C_p$  indicates protein folding.<sup>23-26</sup>

## Chapter 4: Thermodynamic Results and Discussion

### 4.1 Materials

The A $\beta$  peptides used for thermodynamic studies were purchased from W.M. Keck Biotechnology Resource Laboratory at Yale University (New Haven, CT, USA). The peptides received from W.M. Keck Facility were A $\beta$ 16, A $\beta$ 28, A $\beta$ 28(H6A), A $\beta$ 28(H13A), A $\beta$ 28(H14A), Rat A $\beta$ 28. A $\beta$ 16 was received as more than 95% pure peptide and the rest were received as crude peptides. The following crude peptides, A $\beta$ 28, A $\beta$ 28(H6A), A $\beta$ 28(H13A), A $\beta$ 28(H14A), Rat A $\beta$ 28, were purified using high performance liquid chromatography (HPLC) on a standard C<sub>18</sub> preparative column. ACES buffer, copper atomic absorption standard (1% HCl), and other chemicals were purchased from Sigma-Aldrich as more than 99% pure reagents.

### 4.2 Sample Preparation

The peptide solutions were prepared by dissolving approximately 4-10 mg of the purified peptides in 6-6.5 ml of ACES (pH 7.4) with 100 mM NaCl and were spun down to remove undissolved material. The peptide solution concentrations were determined using UV-vis spectroscopy (Thermo Scientific NanoDrop 2000C spectrophotometer) at 276 nm with an extinction coefficient 1,410 M<sup>-1</sup> cm<sup>-1</sup>.<sup>31</sup> The Cu<sup>2+</sup> metal stock solutions were prepared using a copper atomic absorption standard (1% HCl). Different concentrations of 20 mM, 50 mM, and 100 mM ACES (pH=7.4) and 100 mM NaCl were prepared using ACES. The peptide stock solutions and metal stock solutions were diluted using identical buffer (ACES, pH =7.4, and 100 mM NaCl). The approximate concentrations of metal and peptide stock solution were found to be 5 mM and 0.135-0.140 mM respectively. A 2.1mM Cu<sup>2+</sup> metal solution is prepared from the

5mM  $\text{Cu}^{2+}$  stock solution. All the temperature dependent studies were done using 2.1 mM  $\text{Cu}^{2+}$  metal solution and 0.135-0.140 mM peptide solutions, which were prepared using 20 mM ACES (pH 7.4) and 100 mM NaCl.

### **4.3 Isothermal Titration Calorimetry Conditions**

ITC experiments were performed using a MicroCal VP-ITC ultrasensitive titration calorimeter. Temperature dependent experiments were conducted at three different temperatures (10°C, 25°C, and 37°C). For each peptide, titrations were performed in triplicates or quadruplicates to ensure the reproducibility and allow statistical analysis. In a typical ITC experiment, 8 $\mu$ L of metal solution (titrant) was injected into the peptide solution (macromolecule) in cell for 20 s with an interval of 300 s between each injection to allow the system to equilibrate to the baseline. To ensure rapid mixing of the peptide and metal solutions in cell, the stirring speed was maintained at 307 rpm. The conditions were maintained similar for all the injections except for the first injection where only 2 $\mu$ L of metal solution was injected with an interval of 120 s. Titration of metal solution into peptide solution was continued until 3-5 molar equivalents of metal was added to ensure complete saturation of the peptide. The last ten data points were averaged and subtracted from each experimental titration to account for the heat of dilution.

## 4.4 Results and Discussion

### 4.4.1 Buffer Independent Studies

To determine whether ternary complex formation played a role in the binding of  $\text{Cu}^{2+}$  to  $\text{A}\beta$  peptides, titrations were performed in two additional ACES buffer concentrations (50 and 100 mM). A representative ITC integrated data set for the titration of  $\text{Cu}^{2+}$  into  $\text{A}\beta_{16}$  with 20 mM, 50 mM, and 100 mM ACES (pH=7.4) and 100 mM NaCl is shown in Figure 13. It can be observed from Figure 13 that as the ACES concentration increases, the slope becomes more gradual, thus indicating a greater competition for  $\text{Cu}^{2+}$  from the ACES buffer.

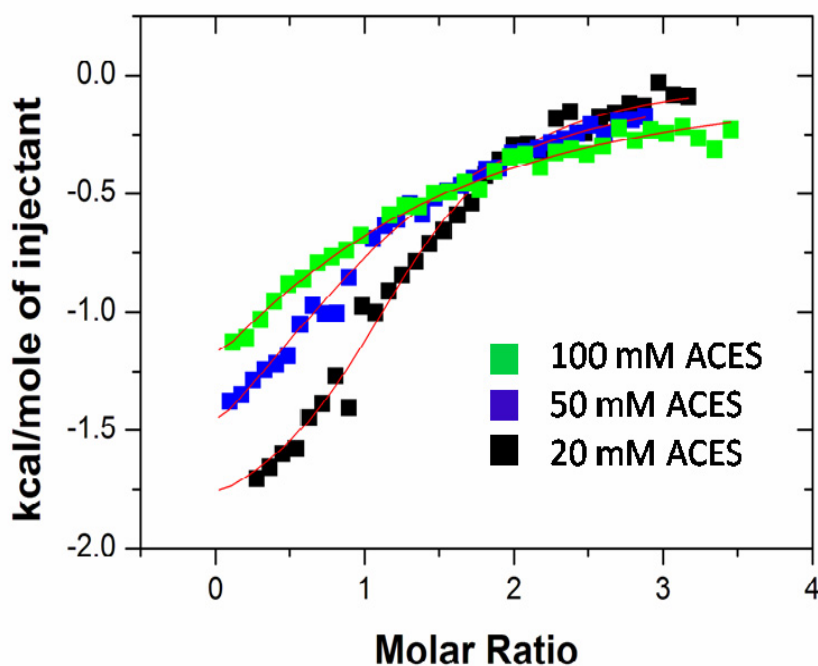


**Figure 13.** ITC integrated data representing the titration of  $\text{Cu}^{2+}$  into  $\text{A}\beta_{16}$  with 20, 50, and 100 mM ACES (pH=7.4). All samples were run at  $37^\circ\text{C}$  and include 100 mM NaCl. Buffer independent binding constants are listed in Table 4.<sup>17</sup>

Fitting the binding isotherms to a “single set of sites” binding model described in chapter 3 provided buffer and pH dependent parameters. Buffer independent binding constants (K) were then calculated using the Eq. 1.<sup>17</sup> K and K<sub>d</sub> obtained for titrations run in 20, 50, and 100 mM ACES are listed in Table 4.<sup>17</sup>

$$K_{M-Peptide} = K_{ITC} \left( 1 + K_{MB} [B] + K_{MB_2} [B]^2 \right) \quad \text{Eq. 1}$$

**Table 4.** Buffer independent K and K<sub>d</sub> values for Aβ16 peptide in 20mM, 50mM, and 100mM ACES (pH 7.4) with 100mM NaCl.<sup>17</sup>

Peptide	[Buffer] (mM)	K (×10 <sup>9</sup> )	K <sub>d</sub> (nM)
Aβ16	20	1.10	0.95
Aβ16	50	1.04	0.96
Aβ16	100	1.06	0.95

The calculated K values for Aβ16 in 50 and 100 mM ACES were within error of values obtained in 20 mM ACES. This consistency in K values for Aβ16 in 20, 50, and 100 mM ACES argues against the formation of ternary complexes. The presence of ternary complexes would result in a difference of condition independent binding constants. Finally, it can be concluded that the buffer independent binding constant values are independent of the concentration of ACES buffer, thus indicating the insignificance of ternary complexes in solution.

#### **4.4.2 Temperature Dependence Studies: Cu<sup>2+</sup> Binding to A $\beta$ 28 and Mutant Peptides**

The binding of Cu<sup>2+</sup> to A $\beta$ 28 and the mutant peptides A $\beta$ 28H6A, A $\beta$ 28H13A and A $\beta$ 28H14A was investigated using ITC at 10°C, 25°C and 37°C. The thermodynamic parameters  $\Delta G$ ,  $\Delta H$ ,  $\Delta S$  and  $\Delta C_p$  were obtained and will be discussed below.

##### **4.4.2.1 Cu<sup>2+</sup> binding to A $\beta$ 28**

Representative binding isotherms for Cu<sup>2+</sup> binding to A $\beta$ 28 at 10°C, 25°C and 37°C are shown in Figure 14. The three thermograms display a single exothermic event centered at a molar ratio of n=1 thus corresponding to the binding of a single Cu<sup>2+</sup> ion to the peptide. All three data sets were fit to a “single set of sites” binding model and the thermodynamic values are presented in Table 5.

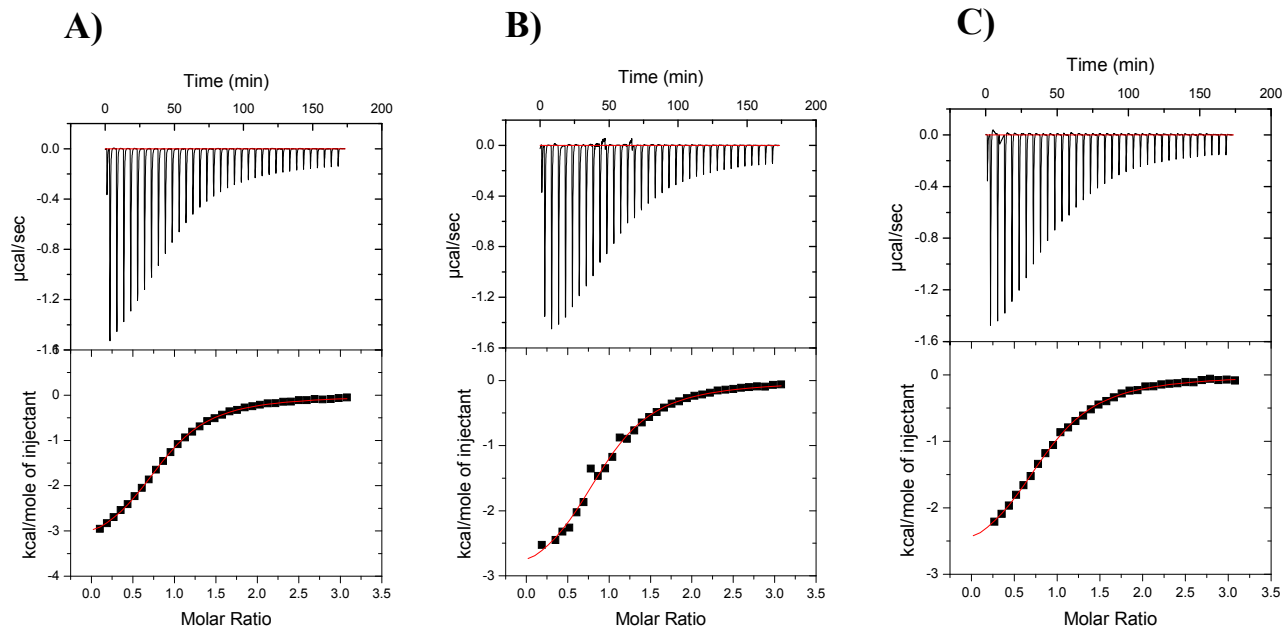


**Figure 14.** Representative ITC data for the titration of 2.1 mM  $\text{Cu}^{2+}$  into 0.140 mM  $\text{A}\beta_{28}$  at A) 10°C, B) 25°C, and C) 37°C. All solutions were in 20 mM ACES (pH=7.4) and 100mM NaCl. Best fit ITC values are listed in Table 5.

From the thermodynamic parameters listed in Table 5, it is observed that  $\Delta G$  is negative, thus indicating a favorable metal binding reaction at all three temperatures. It is also observed that  $\Delta G$  becomes slightly more negative as the temperature increases suggesting that  $\text{Cu}^{2+}$  binding to  $\text{A}\beta_{28}$  becomes more favorable with increasing temperature.

$\Delta H$  of metal binding is exothermic and therefore favorable at all three temperatures. However,  $\Delta H$  of  $\text{Cu}^{2+}$  binding to  $\text{A}\beta_{28}$  becomes more positive and therefore more unfavorable with increasing temperature. This is indicative of either weaker bonding interactions or a disruption in bonding networks such as H-bonding, van der Waals interactions, or hydrophobic interactions.

$\Delta S$  of metal binding is positive and favorable at all three temperatures therefore indicating a favorable reaction. This  $\Delta S$  of  $\text{Cu}^{2+}$  binding becomes more positive and hence more favorable with increasing temperature. This indicates either a release of solvent molecules into the bulk solution upon metal binding that increases at higher temperature or a gain in flexibility in the peptide at higher temperatures.

**Table 5.** Best fit ITC parameters of  $\text{Cu}^{2+}$  into  $\text{A}\beta 28$  at  $10^\circ\text{C}$ ,  $25^\circ\text{C}$ , and  $37^\circ\text{C}$ . The values listed are the mean of four data sets. The standard error values are included in parenthesis.

	<b>10°C</b>	<b>25°C</b>	<b>37°C</b>
<b>N</b>	0.90 ( $\pm 0.03$ )	0.97 ( $\pm 0.10$ )	1.00 ( $\pm 0.10$ )
<b>K (<math>\times 10^4</math>)</b>	4.6 ( $\pm 0.6$ )	5.3 ( $\pm 0.3$ )	4.3 ( $\pm 0.2$ )
<b><math>\Delta H</math> (kcal/mol)</b>	-3.6 ( $\pm 0.2$ )	-3.1 ( $\pm 0.1$ )	-2.9 ( $\pm 0.1$ )
<b><math>\Delta G</math> (kcal/mol)</b>	-6.0 ( $\pm 0.1$ )	-6.4 ( $\pm 0.1$ )	-6.5 ( $\pm 0.2$ )
<b>T<math>\Delta S</math> (kcal/mol)</b>	2.4 ( $\pm 0.2$ )	3.4 ( $\pm 0.1$ )	3.5 ( $\pm 0.1$ )

$\Delta C_p$  for  $\text{Cu}^{2+}$  binding to  $\text{A}\beta 28$  was obtained from a plot of  $\Delta H$  verses temperature. A representative plot of  $\Delta H$  verses temperature for  $\text{Cu}^{2+}$  binding to  $\text{A}\beta 28$  is shown in Figure 15. The  $\Delta C_p$  obtained was the slope of this plot. The averaged  $\Delta C_p$  value calculated was found to be  $25 \pm 3$  cal/mol·T. A positive  $\Delta C_p$  typically indicates the presence of less compact structures in solution with exposed hydrophobic residues. As a result, the  $\Delta S$  with increasing temperature may stem from a gain in flexibility in the peptide accompanying these less compact structures as opposed to a release of solvent molecules in to the bulk solution.

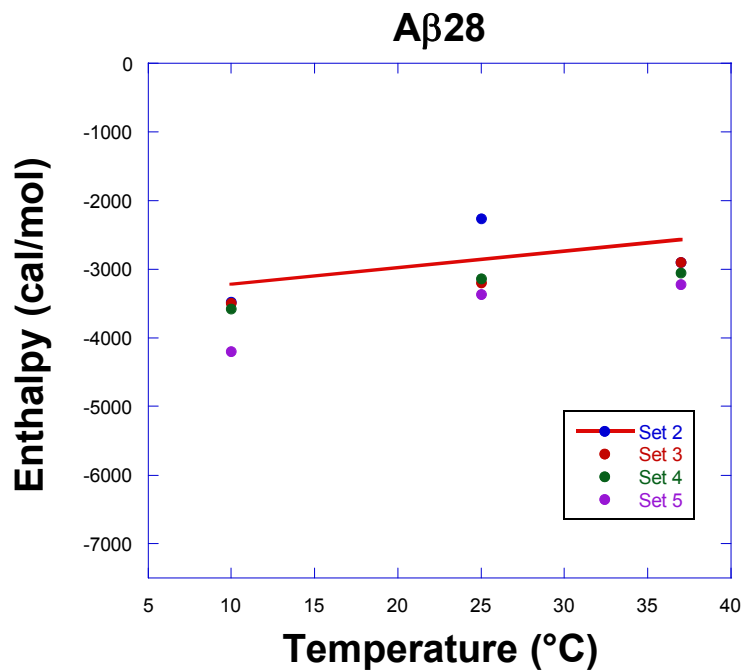


**Figure 15.** A plot of change in enthalpy verses temperature for the binding of 2.1 mM Cu<sup>2+</sup> to A $\beta$ 28 for four sets is shown in the graph. Best fit line is shown for set 2.

#### 4.4.2.2 Cu<sup>2+</sup> binding to A $\beta$ 28H6A

Representative binding isotherms for Cu<sup>2+</sup> binding to A $\beta$ 28H6A at 10°C, 25°C and 37°C are shown in Figure 16. The three thermograms display a single exothermic event centered at a molar ratio of n=1 therefore corresponding to the binding of a single Cu<sup>2+</sup> ion to the peptide as was the case with A $\beta$ 28. All three data sets were fit to a “single set of sites” binding model and the thermodynamic values are presented in Table 6.

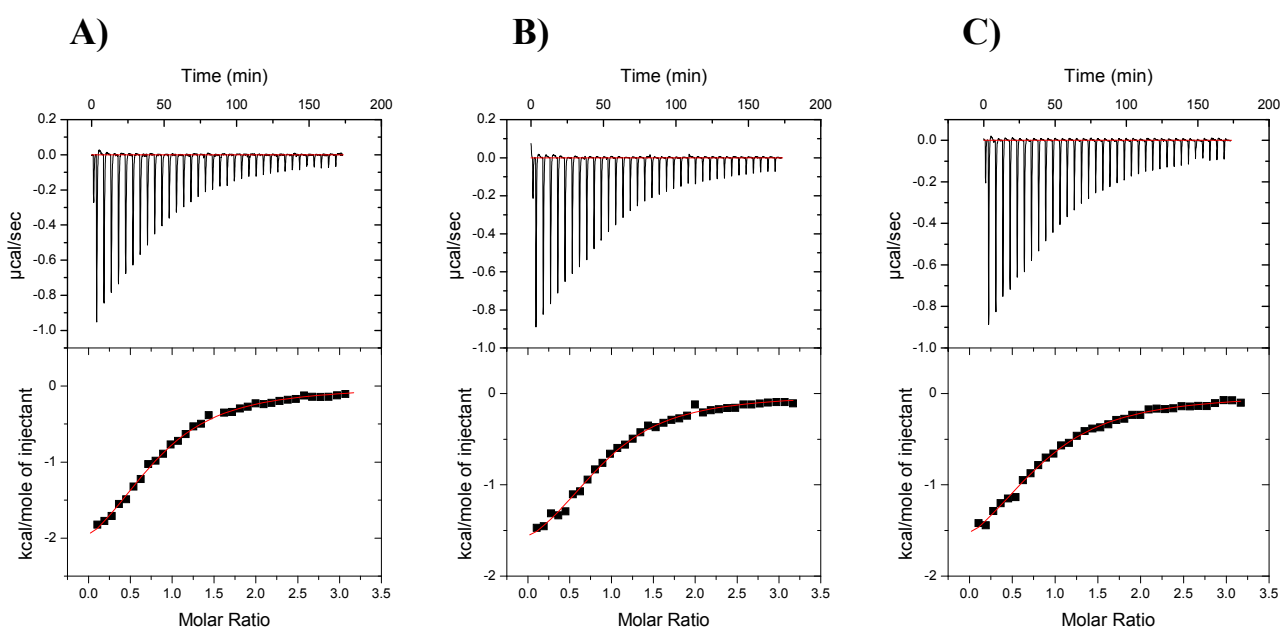


**Figure 16.** Representative ITC data for the titration of 2.1 mM Cu<sup>2+</sup> into 0.140 mM A $\beta$ 28H6A at A) 10°C, B) 25°C, and C) 37°C. All solutions were in 20 mM ACES (pH=7.4) and 100 mM NaCl. Best fit ITC values are listed in Table 6.

The thermodynamic parameters for Cu<sup>2+</sup> binding to A $\beta$ 28H6A listed in Table 6 follow the same trends as those obtained for Cu<sup>2+</sup> binding to A $\beta$ 28. Both the  $\Delta G$  and  $\Delta S$  of metal binding become more favorable with increasing temperature, while the  $\Delta H$  becomes more positive and less favorable.

**Table 6.** Best fit ITC parameters of Cu<sup>2+</sup> into A $\beta$ 28H6A at 10°C, 25°C, and 37°C. The values listed are the mean of three data sets. The standard error values are included in parenthesis.

	10°C	25°C	37°C
<b>N</b>	0.74 ( $\pm 0.04$ )	0.81 ( $\pm 0.10$ )	0.81 ( $\pm 0.04$ )
<b>K (<math>\times 10^4</math>)</b>	2.30 ( $\pm 0.02$ )	2.1 ( $\pm 0.2$ )	2.3 ( $\pm 0.3$ )
<b><math>\Delta H</math> (kcal/mol)</b>	-2.8 ( $\pm 0.1$ )	-2.3 ( $\pm 0.2$ )	-2.2 ( $\pm 0.1$ )
<b><math>\Delta G</math> (kcal/mol)</b>	-5.6 ( $\pm 0.1$ )	-5.9 ( $\pm 0.1$ )	-6.2 ( $\pm 0.1$ )
<b>T<math>\Delta S</math> (kcal/mol)</b>	2.8 ( $\pm 0.1$ )	3.6 ( $\pm 0.2$ )	3.9 ( $\pm 0.1$ )

$\Delta C_p$  for Cu<sup>2+</sup> binding to A $\beta$ 28H6A was obtained from a plot of  $\Delta H$  verses temperature (Figure 17) and found to be  $23 \pm 1$  cal/mol·T. This is similar to the value obtained for metal binding to A $\beta$ 28 and suggests the formation of less compact structures in solution. In general, the larger  $\Delta S$  values and less favorable  $\Delta H$  values suggest structures that are more flexible in solution with overall weaker binding interactions.

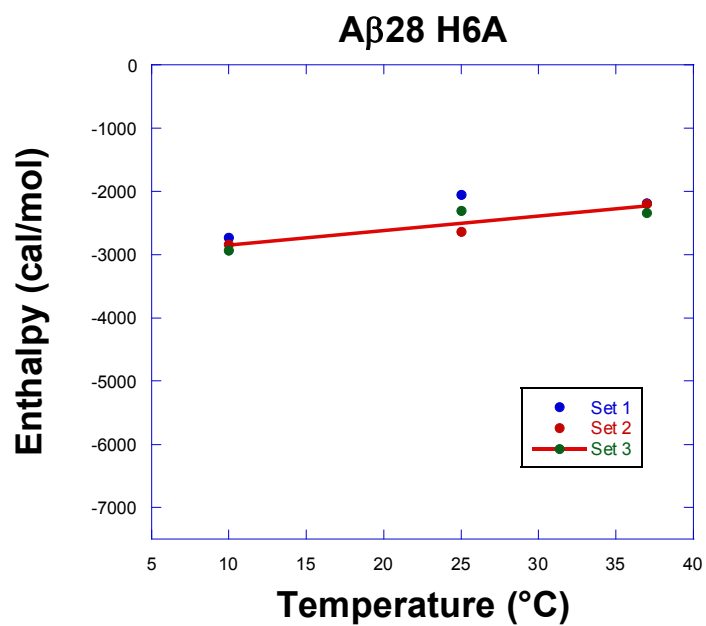


**Figure 17.** A plot of change in enthalpy versus temperature for the binding of 2.1 mM Cu<sup>2+</sup> to A $\beta$ 28H6A for three sets is shown. Best fit line is shown for set 3.

#### 4.4.2.3 Cu<sup>2+</sup> binding to A $\beta$ 28H13A

Representative binding isotherms for Cu<sup>2+</sup> binding to A $\beta$ 28H13A at 10°C, 25°C and 37°C are shown in Figure 18. The three thermograms display a single exothermic event centered at a molar ratio of n=1 therefore corresponding to the binding of a single Cu<sup>2+</sup> ion to the peptide as was the case with A $\beta$ 28 and A $\beta$ 28H6A. All three data sets were fit to a “single set of sites” binding model and the thermodynamic values are presented in Table 7.

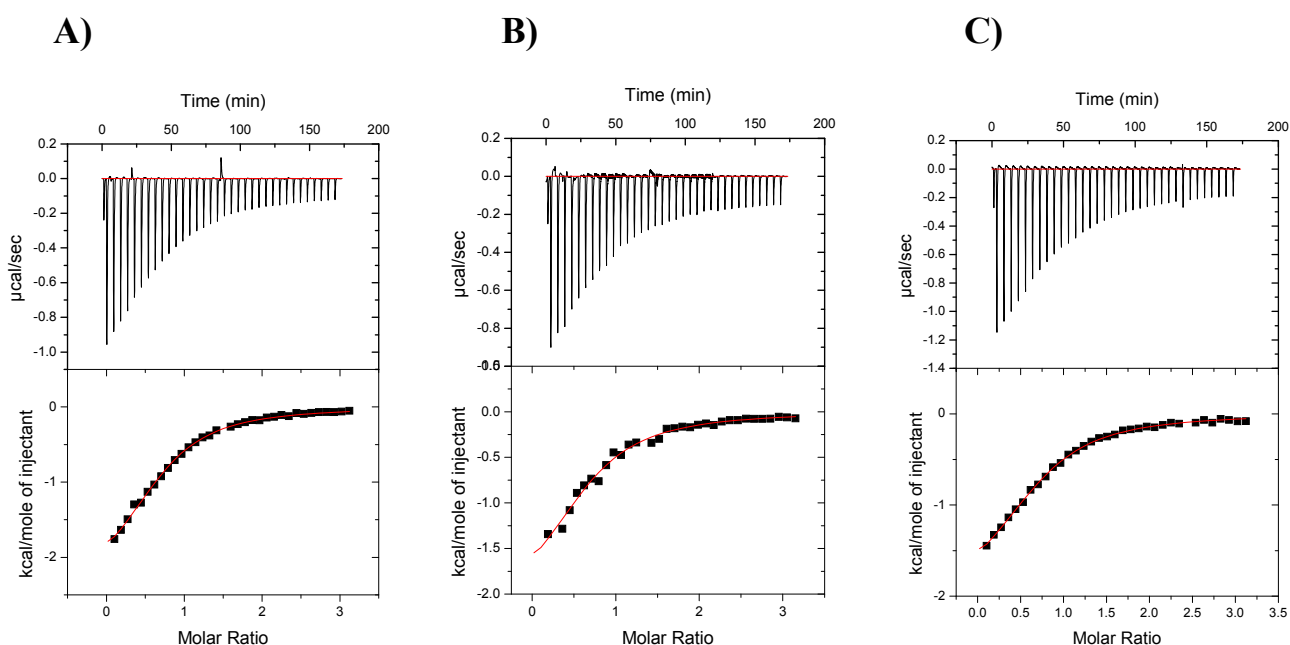


**Figure 18.** Representative ITC data for the titration of 2.1 mM Cu<sup>2+</sup> into 0.140 mM A $\beta$ 28H13A at A) 10°C, B) 25°C, and C) 37°C. All solutions were in 20mM ACES (pH=7.4) and 100 mM NaCl. Best fit ITC values are listed in Table 7.

The thermodynamic parameters for Cu<sup>2+</sup> binding to A $\beta$ 28H6A listed in Table 7 follow the same trends as those obtained for Cu<sup>2+</sup> binding to A $\beta$ 28 and A $\beta$ 28H6A. Both the  $\Delta G$  and  $\Delta S$

of metal binding become more favorable with increasing temperature, while the  $\Delta H$  becomes more positive and less favorable.

**Table 7.** Best fit ITC parameters of  $\text{Cu}^{2+}$  into A $\beta$ 28H13A at 10°C, 25°C, and 37°C. The values listed are the mean of three data sets. The standard error values are included in parenthesis.

	10°C	25°C	37°C
<b>N</b>	0.81 ( $\pm 0.10$ )	0.74 ( $\pm 0.10$ )	0.79 ( $\pm 0.04$ )
<b>K (<math>\times 10^4</math>)</b>	2.7 ( $\pm 0.3$ )	3.0 ( $\pm 0.3$ )	3.5 ( $\pm 0.7$ )
<b><math>\Delta H</math> (kcal/mol)</b>	-2.5 ( $\pm 0.1$ )	-2.3 ( $\pm 0.1$ )	-2.0 ( $\pm 0.1$ )
<b><math>\Delta G</math> (kcal/mol)</b>	-5.7 ( $\pm 0.1$ )	-6.1 ( $\pm 0.1$ )	-6.4 ( $\pm 0.1$ )
<b>T<math>\Delta S</math> (kcal/mol)</b>	3.2 ( $\pm 0.1$ )	3.8 ( $\pm 0.1$ )	4.4 ( $\pm 0.2$ )

$\Delta C_p$  for  $\text{Cu}^{2+}$  binding to A $\beta$ 28H13A was also obtained from a plot of  $\Delta H$  verses temperature (Figure 19) and found to be  $17 \pm 1$  cal/mol·T. This value is different and smaller than the  $\Delta C_p$  values obtained for metal binding to A $\beta$ 28 and A $\beta$ 28H6A. This suggests the formation of species that are more compact with less exposed hydrophobic residues than A $\beta$ 28 and A $\beta$ 28H6A.

The larger  $\Delta S$  values observed for  $\text{Cu}^{2+}$  binding to A $\beta$ 28 as compared to wild-type AB28 suggest either more flexible coordination complexes in solution or a larger release of water molecules into the bulk solution resulting from the burial of hydrophobic residues upon metal binding. The less favorable  $\Delta H$  values obtained for metal binding to the mutant peptides as compared to that observed for the wild-type are indicative to weaker binding interactions. This may be due to the removal of a potential metal binding ligand.

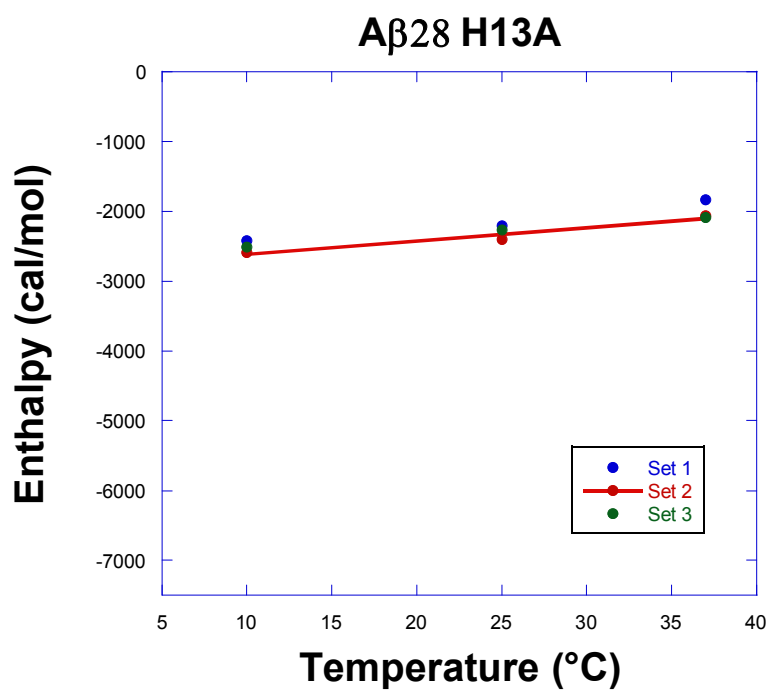


**Figure 19.** A plot of change in enthalpy verses temperature for the binding of 2.1 mM  $\text{Cu}^{2+}$  to A $\beta$ 28H13A for three sets is shown in the graph. Best fit line is shown for set 2.

#### 4.4.2.4 Cu<sup>2+</sup> binding to A $\beta$ 28H14A

Representative binding isotherms for Cu<sup>2+</sup> binding to A $\beta$ 28H14A at 10°C, 25°C and 37°C are shown in Figure 20. The three thermograms display a single exothermic event centered at a molar ratio of n=1 therefore corresponding to the binding of a single Cu<sup>2+</sup> ion to the peptide as was the case with A $\beta$ 28, A $\beta$ 28H6A and A $\beta$ 28H13A. All three data sets were fit to a “single set of sites” binding model and the thermodynamic values are presented in Table 8.

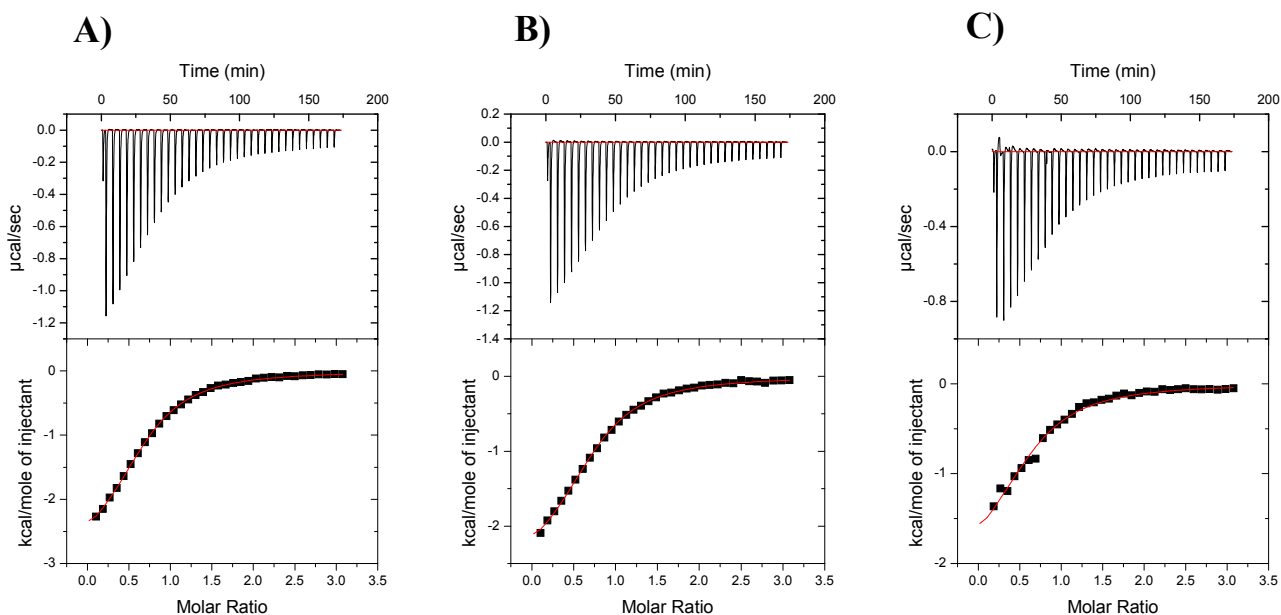


**Figure 20.** Representative ITC data for the titration of 2.1 mM Cu<sup>2+</sup> into 0.140 mM A $\beta$ 28H14A at A) 10°C, B) 25°C, and C) 37°C. All solutions were in 20 mM ACES (pH 7.4) and 100 mM NaCl. Best fit ITC values are listed in Table 8.

From the listed thermodynamic parameters in Table 8, it can be observed that the  $\Delta G$  is negative for all temperatures, thus indicating a favorable metal binding reaction. Also, it is observed that the  $\Delta G$  value increases slightly as the temperature increases as was seen with the

previous peptides. Both the  $\Delta S$  and  $\Delta H$  of metal binding to AB28H14A follow similar trends observed with the previous peptides. The  $\Delta S$  becomes more favorable with increasing temperature while the  $\Delta H$  becomes more positive and hence less favorable.

**Table 8.** Best fit ITC parameters of  $\text{Cu}^{2+}$  into A $\beta$ 28H14A at 10°C, 25°C, and 37°C. The values listed are the mean of three data sets. The standard error values are included in parenthesis.

	10°C	25°C	37°C
<b>N</b>	0.77 ( $\pm 0.10$ )	0.81 ( $\pm 0.10$ )	0.76 ( $\pm 0.10$ )
<b>K (<math>\times 10^4</math>)</b>	4.3 ( $\pm 0.3$ )	4.4 ( $\pm 0.6$ )	5.0 ( $\pm 1.2$ )
<b><math>\Delta H</math> (kcal/mol)</b>	-3.0 ( $\pm 0.1$ )	-2.6 ( $\pm 0.1$ )	-2.2 ( $\pm 0.1$ )
<b><math>\Delta G</math> (kcal/mol)</b>	-6.0 ( $\pm 0.1$ )	-6.3 ( $\pm 0.1$ )	-6.7 ( $\pm 0.2$ )
<b>T<math>\Delta S</math> (kcal/mol)</b>	3.0 ( $\pm 0.1$ )	3.7 ( $\pm 0.1$ )	4.5 ( $\pm 0.2$ )

$\Delta C_p$  for  $\text{Cu}^{2+}$  binding to A $\beta$ 28H14A was obtained from a plot of  $\Delta H$  verses temperature (Figure 21).  $\Delta C_p$  was found to be  $30 \pm 1$  cal/mol·T. This value is more positive than  $\Delta C_p$  values obtained for A $\beta$ 28 and the other mutant peptides thus suggesting the formation of more unfolded and less compact structures in solution. The greater entropies of metal binding obtained versus wild-type suggest that these structures are more flexible in solution with greater conformational degrees of freedom.

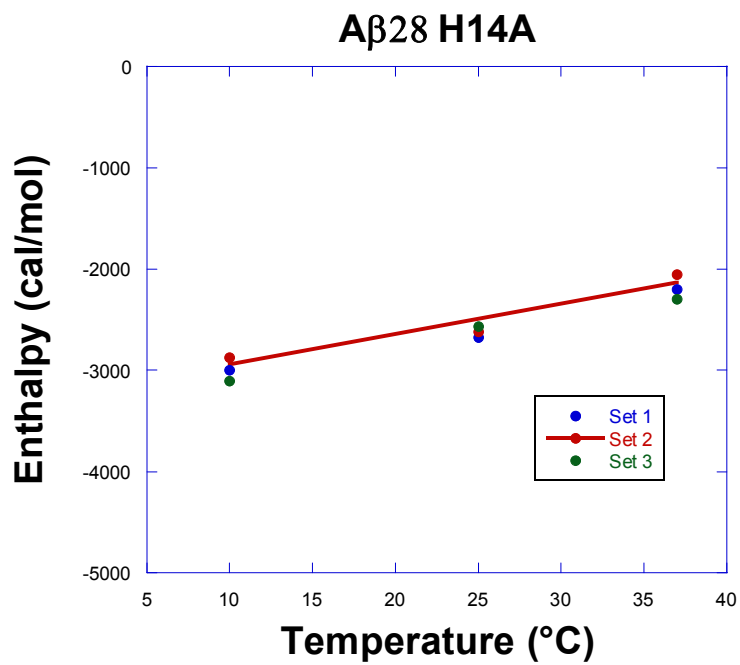


**Figure 21.** A plot of change in enthalpy verses temperature for the binding of 2.1 mM  $\text{Cu}^{2+}$  to A $\beta$ 28H14A for three sets is shown in the graph. Best fit line is shown for set 2.

#### 4.4.3. Temperature Dependence Studies: $\text{Cu}^{2+}$ Binding to Rat A $\beta$ 28

Representative binding isotherms for  $\text{Cu}^{2+}$  binding to rat A $\beta$ 28 at 10°C, 25°C and 37°C are shown in Figure 22. The three thermograms display a single exothermic event centered at a molar ratio of  $n=1$  thus corresponding to the binding of a single  $\text{Cu}^{2+}$  ion to the peptide as was the case with A $\beta$ 28 and the mutant peptides. All three data sets were fit to a “single set of sites” binding model and the thermodynamic values are presented in Table 9.

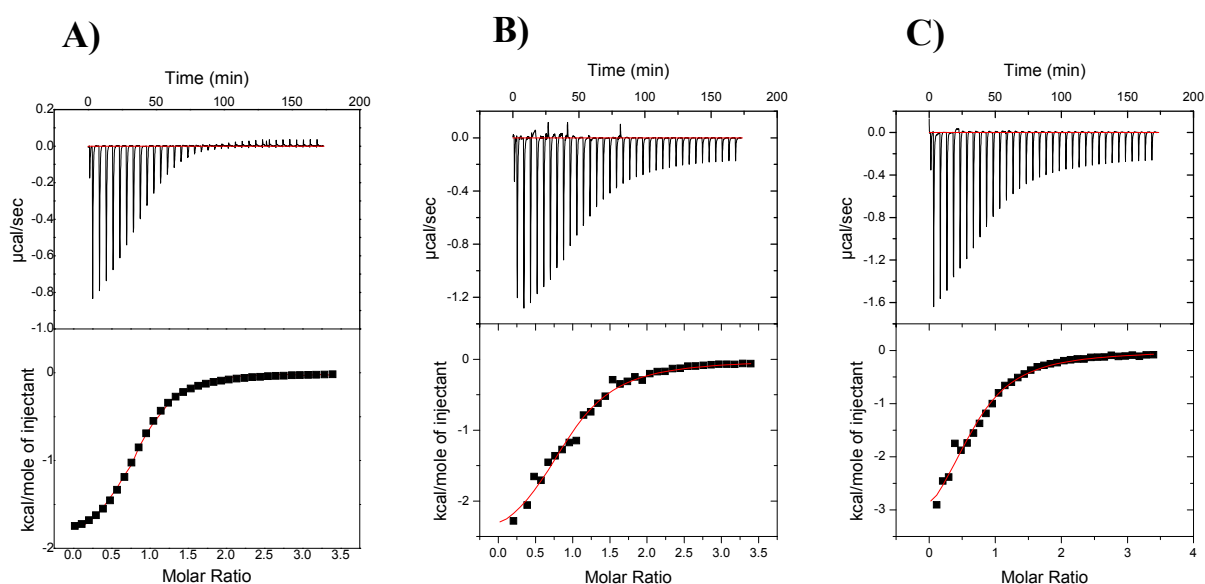


**Figure 22.** Representative ITC data for the titration of 2.1 mM  $\text{Cu}^{2+}$  into 0.140 mM Rat A $\beta$ 28 at A) 10°C, B) 25°C, and C) 37°C. All solutions were in 20 mM ACES (pH=7.4) and 100 mM NaCl. Best fit ITC values are listed in Table 9.

From the thermodynamic parameters listed in Table 9, it is observed that the  $\Delta G$  is negative, thus indicating a favorable metal binding reaction at all three temperatures. This is similar to the  $\Delta G$  values observed for  $\text{Cu}^{2+}$  binding to A $\beta$ 28 and the mutant peptides.

Interestingly, the  $\Delta G$  does not change with changing temperature and does not reveal a temperature dependence as was the case with the wild-type and mutant peptides.

The  $\Delta H$  of  $\text{Cu}^{2+}$  binding to rat A $\beta$ 28 is more favorable than  $\text{Cu}^{2+}$  binding to wild-type and mutant peptides. In addition, although  $\Delta H$  of  $\text{Cu}^{2+}$  binding to rat A $\beta$ 28 is exothermic and therefore favorable at all three temperatures, the  $\Delta H$  becomes more negative and therefore more favorable with increasing temperature. This is in direct contrast to the decrease in  $\Delta H$  observed for wild-type and A $\beta$  peptides. These values are indicative of either stronger bonding interactions or a strengthening in bonding networks such as H-bonding, van der Waals interactions, or hydrophobic interactions occurring upon metal binding to rat A $\beta$  with increasing temperatures.

$\Delta S$  of  $\text{Cu}^{2+}$  binding to rat A $\beta$ 28 is positive and favorable at all three temperatures but is less favorable than what was observed for the wild-type and mutant peptides. This indicates that the  $\text{Cu}^{2+}$  complexes formed with the rat peptide are more structurally rigid and/or more compact than the wild-type or mutant forms. Furthermore, the  $\Delta S$  of  $\text{Cu}^{2+}$  binding becomes less positive and hence more unfavorable with increasing temperature. This indicates either a release of fewer solvent molecules into the bulk solution upon metal binding with increasing temperature or a decrease in the flexibility of the metal-peptide complex at higher temperatures.

**Table 9.** Best fit ITC parameters of Cu<sup>2+</sup> into Rat A $\beta$ 28 at 10°C, 25°C, and 37°C. The values listed are the mean of two data sets. The standard error values are included in parenthesis.

	10°C	25°C	37°C
<b>N</b>	1.06 ( $\pm 0.20$ )	1.04 ( $\pm 0.10$ )	0.95 ( $\pm 0.02$ )
<b>K (<math>\times 10^4</math>)</b>	8 ( $\pm 2$ )	3.9 ( $\pm 0.6$ )	2.8 ( $\pm 0.2$ )
<b><math>\Delta H</math> (kcal/mol)</b>	-1.9 ( $\pm 0.1$ )	-2.8 ( $\pm 0.1$ )	-3.8 ( $\pm 0.1$ )
<b><math>\Delta G</math> (kcal/mol)</b>	-6.3 ( $\pm 0.1$ )	-6.3 ( $\pm 0.1$ )	-6.3 ( $\pm 0.1$ )
<b>T<math>\Delta S</math> (kcal/mol)</b>	4.4 ( $\pm 0.1$ )	3.4 ( $\pm 0.1$ )	2.4 ( $\pm 0.1$ )

$\Delta C_p$  for Cu<sup>2+</sup> binding to rat A $\beta$ 28 was obtained from a plot of  $\Delta H$  verses temperature. A representative plot of  $\Delta H$  verses temperature for Cu<sup>2+</sup> binding to rat A $\beta$ 28 is shown in Figure 23.  $\Delta C_p$  obtained was the slope of this plot. The averaged  $\Delta C_p$  value was found to be  $-71 \pm 1$  cal/mol·T. This value is completely opposite in sign to what was found for the wild-type and mutant peptides.

A negative  $\Delta C_p$  typically indicates the presence of more compact structures in solution with less exposed hydrophobic residues. As a result, this is typically accompanied by the release of water molecules into the bulk solution and an increase in  $\Delta S$  with increasing temperature. Since this was not observed in the data, a less positive  $\Delta S$  suggests more rigid structures with more constrained bonds and therefore less conformational degrees of freedom. This also supports a more compact metal-peptide structure.

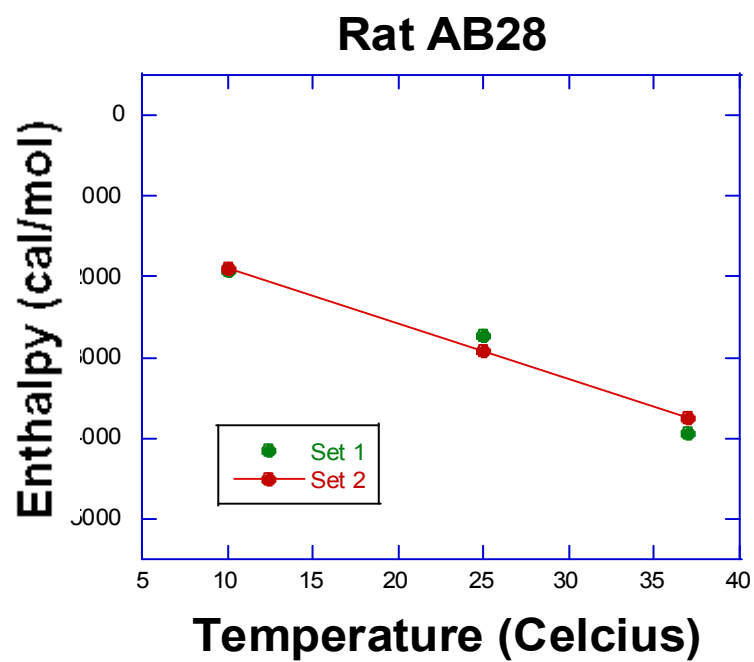


**Figure 23.** A plot of change in enthalpy verses temperature for the binding of 2.1 mM  $\text{Cu}^{2+}$  to Rat A $\beta$ 28 for two sets is shown in the graph. Best fit line is shown for set 2.

#### 4.5 Temperature Dependence Studies: Discussion

In this study, it can be observed that the thermodynamic parameter values for  $\text{Cu}^{2+}$  binding to wild type and mutant type A $\beta$ 28 peptides at 37°C are within error with the previously obtained values in Spuches lab. The  $\Delta C_p$  values are calculated for wild type and mutant type A $\beta$ 28 peptides and listed in Table 10.

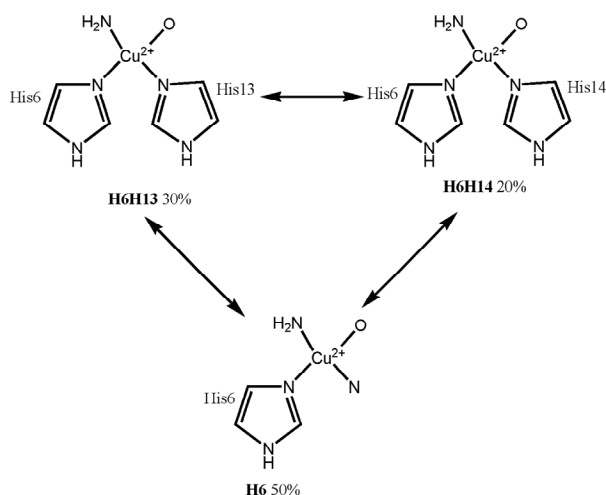
**Table 10.** Heat capacity values for  $\text{Cu}^{2+}$  binding to wild type, mutant type A $\beta$ 28 peptide and Rat A $\beta$ 28 peptide. Thermodynamic parameters values for  $\text{Cu}^{2+}$  binding to peptides at 37°C.

Peptide	$\Delta C_p$ (cal/mol·T)	$\Delta G$ (kcal/mol) @ 37°C	$\Delta H$ (kcal/mol) @ 37°C	T $\Delta S$ (kcal/mol) @ 37°C
A $\beta$ 28	25±3	-6.5 (±0.1)	-3.0 (±0.1)	3.5 (±0.1)
A $\beta$ 28 H6A	23±1	-6.2 (±0.1)	-2.2 (±0.1)	3.9 (±0.1)
A $\beta$ 28 H13A	17±1	-6.4 (±0.1)	-2.0 (±0.1)	4.3 (±0.1)
A $\beta$ 28 H14A	29±1	-6.6 (±0.1)	-2.2 (±0.1)	4.4 (±0.1)
Rat A $\beta$ 28	-71±1	-6.3 (±0.1)	-3.8 (±0.1)	2.5 (±0.1)

Our original goal was to explain why metal binding to the mutants resulted in more favorable  $\Delta S$  than binding to the wild type. We expected that the answers lied in the structures that were formed in solution and determining the  $\Delta C_p$  would provide evidence to explain this. According to our goal we expected that the mutants would provide more compact structures in solution, indicative of a more negative  $\Delta C_p$  verses wild type. But, this trend did not emerge, in fact we found similar values for A $\beta$ 28 and A $\beta$ 28H14A indicating similar structures, and less positive  $\Delta C_p$  values for A $\beta$ 28H13A and A $\beta$ 28H6A indicating more compact structures. Therefore, the greater  $\Delta S$  must stem from more flexible species with greater conformational degrees of freedom.

While the  $\Delta C_p$  data obtained for A $\beta$ 28 and mutant peptides did not reveal interesting trends, the large difference in  $\Delta C_p$  observed for Cu<sup>2+</sup> binding to A $\beta$ 28 and Rat A $\beta$ 28 was very intriguing.

**A)**



**B)**

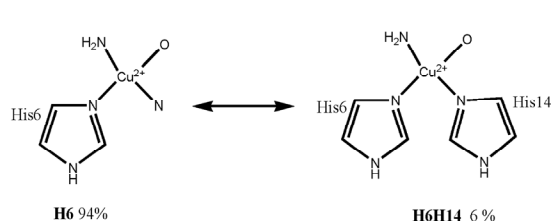


**Figure 24.** Proposed Cu<sup>2+</sup> coordination for A) Human and B) Rat A $\beta$ 16 at pH 7.4, 37°C, and 0.16 M ionic strength.<sup>27</sup>

Human and Rat A $\beta$  peptide differ in the presence of three specific substitutions in the primary amino acid sequence: R5G, Y10F, and H13R. Simon and coworkers have recently deduced the primary coordination spheres of Cu<sup>2+</sup> binding to both Human and Rat A $\beta$ 16.<sup>27</sup> Figure 24 shows the Cu<sup>2+</sup> coordination spheres for both Human A $\beta$ 16 and Rat A $\beta$ 16 at pH 7.4, 37°C as determined by the Simon group. The thermodynamic and spectroscopic analyses revealed the presence of three Cu<sup>2+</sup> coordination spheres, **H6** (50%), **H6H13** (30%), and **H6H14** (20%), in Human A $\beta$ 16 and the presence of predominantly one Cu<sup>2+</sup> coordination sphere, **H6** (94%), in Rat A $\beta$ 16. The thermodynamic properties for Cu<sup>2+</sup> binding to **H6H14** are similar for human and Rat A $\beta$ 16, while the properties for Cu<sup>2+</sup> binding to **H6** are quite different for the two peptides with Rat **H6** exhibiting approximately 6 times the affinity for Cu<sup>2+</sup> as the human **H6**.

Furthermore, the Simon group determined that the single mutation, R5G, reproduced the same quantitative difference in  $\text{Cu}^{2+}$  coordination to Human and Rat **H6**, which was further supported by CD studies. In addition aggregation assays showed that  $\text{Cu}^{2+}$  induced aggregation of human  $\text{A}\beta_{40}$  (R5G) is similar to that of the Rat  $\text{A}\beta_{40}$  peptide.<sup>27</sup> This led the Simon group to propose that the single mutation R5G is responsible for the lack of fibril formation in the Rat  $\text{A}\beta$  peptide.

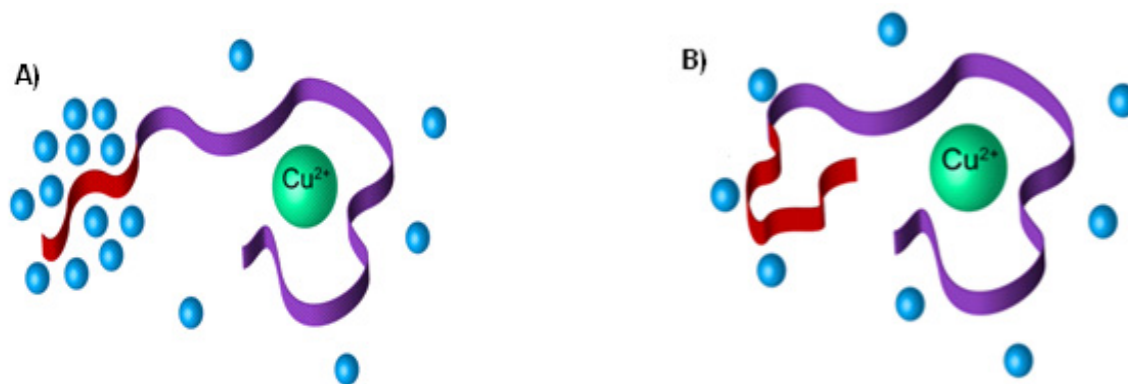


**Figure 25.** Cartoon representation of  $\text{Cu}^{2+}$  bound to A) Human  $\text{A}\beta_{28}$  peptide and B) Rat  $\text{A}\beta_{28}$  peptide. Red patch represents a hydrophobic patch in both the peptides. Each cartoon represents an “average”  $\text{Cu}^{2+}$ –peptide structure in solution and highlights the ordered water molecules surrounding the hydrophobic residues. The figure was generated with Adobe Illustrator CS4.<sup>17</sup>

From the listed  $\Delta C_p$  values in Table 10, we observed a positive  $\Delta C_p$  value for Human  $\text{A}\beta_{28}$  peptide and a negative  $\Delta C_p$  value for Rat  $\text{A}\beta_{28}$  peptide. According to this study, we can conclude that a positive  $\Delta C_p$  value for Human  $\text{A}\beta_{28}$  indicates less compact structures with more exposed hydrophobic residues in solution and a negative  $\Delta C_p$  value for Rat  $\text{A}\beta_{28}$  indicates more compact structures with buried hydrophobic residues as shown in Figure 25. We expand on data from the Simon group by suggesting that the R5G mutation stabilizes the **H6** coordination sphere

and that this coordination results in a more overall compact structure with non-exposed hydrophobic residues.

Our proposed model of  $\text{Cu}^{2+}$  binding may also explain the lack of significant fibril formation in the Rat  $\text{A}\beta$  peptide. Previous FTIR studies of  $\text{A}\beta_{42}$  fibril formation have shown typical parallel  $\beta$ -sheet features, characterized by a maximum of absorbance at  $1630\text{ cm}^{-1}$  in the amide I region.<sup>32</sup> Hydrophobic interactions are proposed to facilitate the formation of these  $\beta$ -sheet structures. Thus, according to our study it suggests that parallel  $\beta$ -sheet fibril formation may be inhibited in Rat  $\text{A}\beta_{28}$  because of the lack of an exposed hydrophobic patch (Figure 26).



**Figure 26.** Parallel  $\beta$ -sheet A) Fibril formation in human  $\text{A}\beta_{28}$  peptide B) No fibril formation in Rat  $\text{A}\beta_{28}$  peptide.<sup>32</sup>

## 4.6 Overall Conclusions

In our study, the buffer independent binding constant values are independent of the concentration of ACES buffer, thus confirming the insignificance of the formation of ternary complexes. The comparison of the  $\Delta C_p$  of  $\text{Cu}^{2+}$  binding to wild type and mutant type A $\beta$ 28 peptides suggests the conclusion that the  $\Delta C_p$  values are similar for  $\text{Cu}^{2+}$  binding to A $\beta$ 28 and A $\beta$ 28H14A, thus indicating similar structures. In addition, it shows less positive  $\Delta C_p$  values for  $\text{Cu}^{2+}$  binding to A $\beta$ H6A and A $\beta$ 28H13A, thus indicating more compact structures. Most importantly, the negative  $\Delta C_p$  observed for  $\text{Cu}^{2+}$  binding to Rat A $\beta$ 28 indicates a more compact structure in solution with buried hydrophobic residues. This suggests that fibril formation may be inhibited in Rat A $\beta$ 28 because of an unexposed hydrophobic patch that is not accessible to form fibrils.

## 4.7 Future Studies

Future studies will include other techniques to study the extent of fibril formation upon  $\text{Cu}^{2+}$  binding to the peptides. Simon and group have performed aggregation assays to understand the effect of  $\text{Cu}^{2+}$  on the aggregation of human A $\beta$ 40 and rat A $\beta$ 40.<sup>27</sup> Similar aggregation assays can be performed on wild type and mutant type peptides to see if there is a correlation between heat capacity and metal induced aggregation.

Future studies also include obtaining heat capacity values for  $\text{Cu}^{2+}$  binding to human A $\beta$ 28 and mutated A $\beta$ 28 peptides (R5G, Y10F and H13R). These three mutations are similar to the three specific substitutions in rat peptides. Therefore these heat capacity studies may provide further insight into the differences between human and rat peptide.

## References

- (1) Alzheimer's Association [http://www.alz.org/alzheimers\\_disease\\_facts\\_figures.asp](http://www.alz.org/alzheimers_disease_facts_figures.asp) (accessed 20 March, 2008).
- (2) Rogaeva, E. The solved and unsolved mysteries of the genetics of early-onset Alzheimer's disease. *NeuroMolecular Medicine* **2002**, *2*, 1-10.
- (3) Cherny, R. A.; Atwood, C. S.; Xilinas, M. E.; Gray, D. N.; Jones, W. D.; McLean, C. A.; Barnham, K. J.; Volitakis, I.; Fraser, F. W.; Kim, Y.; Huang, X.; Goldstein, L. E.; Moir, R. D.; Lim, J. T.; Beyreuther, K.; Zheng, H.; Tanzi, R. E.; Masters, C. L.; Bush, A. I. Treatment with a Copper-Zinc Chelator Markedly and Rapidly Inhibits  $\beta$ -Amyloid Accumulation in Alzheimer's Disease Transgenic Mice. *Neuron* **2001**, *30*, 665-676.
- (4) Reitz, C. Alzheimer's Disease and the Amyloid Cascade Hypothesis: A Critical Review. *International Journal of Alzheimer's Disease* **2012**, *2012* (2012), 11-  
doi:10.1155/2012/369808.
- (5) Karran, E.; Mercken, M.; Strooper, D. B. The amyloid cascade hypothesis for Alzheimer's disease: an appraisal for the development of therapeutics. *Nature Reviews Drug Discovery* **2011**, *10*, 698-712-doi:10.1038/nrd3505.
- (6) [http://www.alz.org/braintour/plaques\\_tangles.asp](http://www.alz.org/braintour/plaques_tangles.asp)
- (7) Kepp, K. P. Bioinorganic Chemistry of Alzheimer's Disease. *Chem. Rev.* **2012**, *112*, 5193-5239.
- (8) Faller, P.; Hureau, C. Bioinorganic chemistry of copper and zinc ions coordinated to amyloid-beta peptide. *Dalton Trans.* **2009**, 1080-1094.
- (9) Masters, C. L.; Multhaup, G.; Simms, G.; Pottgiesser, J.; Martins, R. N.; Beyreuther, K. Neuronal Origin of a Cerebral Amyloid - Neurofibrillary Tangles of Alzheimers-Disease Contain the Same Protein as the Amyloid of Plaque Cores and Blood-Vessels. *EMBO J.* **1985**, *4*, 2757-2763.
- (10) Glenner, G. G. Amyloidosis - Implications in Alzheimers-Disease and Other Diseases. *Ann. Pathol.* **1981**, *1*, 105-108.
- (11) Bush, A. I. The metallobiology of Alzheimer's disease. *Trends Neurosci.* **2003**, *26*, 207-214.
- (12) Kang, J.; Lemaire, H. G.; Unterbeck, A.; Salbaum, J. M.; Masters, C. L.; Grzeschik, K. H.; Multhaup, G.; Beyreuther, K.; Mullerhill, B. The Precursor of Alzheimers-Disease Amyloid-A4 Protein Resembles a Cell-Surface Receptor. *Nature* **1987**, *325*, 733-736.

- (13) Lovell, M. A.; Robertson, J. D.; Teesdale, W. J.; Campbell, J. L.; Markesbery, W. R. Copper, iron and zinc in Alzheimer's disease senile plaques. *J. Neurol. Sci.* **1998**, *158*, 47-52.
- (14) Chen, W.; Liao, Y.; Yu, H.; Cheng, I. H.; Chen, Y. Distinct Effects of Zn(II), Cu(II), Fe(II), and Al(II) on Amyloid-beta Stability, Oligomerization, and Aggregation. *J. Biol. Chem.* **2011**, *286*, 9646-9656.
- (15) Tougu, V.; Tiiman, A.; Palumaa, P. Interactions of Zn(II) and Cu(II) ions with Alzheimer's amyloid-beta peptide. Metal ion binding, contribution to fibrillization and toxicity. *Metallomics* **2011**, *3*, 250-261.
- (16) Dong, J.; Atwood, C. S.; Anderson, V. E.; Siedlak, S. L.; Smith, M. A.; Perry, G.; Carey, P. R. Metal binding and oxidation of amyloid-beta within isolated senile plaque cores: Raman microscopic evidence. *Biochemistry* **2003**, *42*, 2768-2773.
- (17) Sacco, C.; Skowronsky, R.; Gade, S.; Kenney, J.; Spuches, A. Calorimetric investigation of copper(II) binding to A $\beta$  peptides: thermodynamics of coordination plasticity. *Journal of Biological Inorganic Chemistry* **2012**, *17*, 531-541.
- (18) Grosseohme, N.; Spuches, A.; Wilcox, D. Application of isothermal titration calorimetry in bioinorganic chemistry. *Journal of Biological Inorganic Chemistry* **2010**, *15*, 1183-1191.
- (19) Hong, L.; Bush, W. D.; Hatcher, L. Q.; Simon, J. Determining Thermodynamic Parameters from Isothermal Calorimetric Isotherms of the Binding of Macromolecules to Metal Cations Originally Chelated by a Weak Ligand. *J Phys Chem B* **2008**, *112*, 604-611.
- (20) Rozga, M.; Kloniecki, M.; Dadlez, M.; Bal, W. A Direct Determination of the Dissociation Constant for the Cu(II) Complex of Amyloid beta 1-40 Peptide. *Chem. Res. Toxicol.* **2010**, *23*, 336-340.
- (21) Rozga, M.; Protas, A. M.; Jablonowska, A.; Dadlez, M.; Bal, W. The Cu(II) complex of A beta 40 peptide in ammonium acetate solutions. Evidence for ternary species formation. *Chem. Commun.* **2009**, 1374-1376.
- (22) Cooper, A. Protein Heat Capacity: An Anomaly that Maybe Never Was. *J. Phys. Chem. Lett.* **2010**, *1*, 3298-3304.
- (23) Privalov, P. L.; Makhatadze, G. I. Contribution of hydration and non-covalent interactions to the heat capacity effect on protein unfolding. *J. Mol. Biol.* **1992**, *224*, 715-723.
- (24) Sturtevant, J. M. Heat capacity and entropy changes in processes involving proteins. *Proceedings of the National Academy of Sciences* **1977**, *74*, 2236-2240.
- (25) Gómez, J.; Hilser, V. J.; Xie, D.; Freire, E. The heat capacity of proteins. *Proteins: Structure, Function, and Bioinformatics* **1995**, *22*, 404-412.

- (26) Murphy, K. P.; Gill, S. J. Solid model compounds and the thermodynamics of protein unfolding. *J. Mol. Biol.* **1991**, *222*, 699-709.
- (27) Hong, L.; Carducci, T. M.; Bush, W. D.; Dudzik, C. G.; Millhauser, G. L.; Simon, J. D. Quantification of the Binding Properties of Cu<sup>2+</sup> to the Amyloid Beta Peptide: Coordination Spheres for Human and Rat Peptides and Implication on Cu<sup>2+</sup>-Induced Aggregation. *J. Phys. Chem. B* **2010**, *114*, 11261-11271.
- (28) ULTRASENSITIVE CALORIMETRY FOR THE LIFE SCIENCES  
<http://www.microcal.com/technology/itc.asp> (accessed 11/1/2012, 2012).
- (29) Figure courtesy of the Wilcox Group, Dartmouth College, **2008**.
- (30) MicroCal, L. ITC Data Analysis in Origin® Tutorial Guide Version 7. *MAUI30010 REV D* **2004**, F-4, F-4.
- (31) Gill, S. C.; von Hippel, P. H. Calculation of protein extinction coefficients from amino acid sequence data. *Anal. Biochem.* **1989**, *182*, 319-326.
- (32) Cerf, E.; Sarroukh, R.; Tamamizu-Kato, S.; Breydo, L.; Derclaye, S.; Dufrene, Y. F.; Narayanaswami, V.; Goormaghtigh, E.; Ruyschaert, J. M.; Raussens, V. Antiparallel beta-sheet: a signature structure of the oligomeric amyloid beta-peptide. *Biochem. J.* **2009**, *421*, 415-423.